A THESIS FOR THE DEGREE OF DOCTOR OF PHILOSOPHY

Fabrication and Characterization of Printed Sensors based on Nano-composite Materials

Shahid Aziz

Department of Mechatronics Engineering

GRADUATE SCHOOL

JEJU NATIONAL UNIVERSITY

2017.02.

Department of Mechatronics Engineering
GRADUATE SCHOOL
JEJU NATIONAL UNIVERSITY

2017. 02

Fabrication and Characterization of Printed Sensors based on Nano-composite Materials

Shahid Aziz

(Supervised by Professor Kyung Hyun Choi)

A thesis submitted in partial fulfillment of the requirement for
the degree of Doctor of Philosophy

2017. 02

The thesis has been examined and approved.

Jong Hwan Lim
Thesis Director, Jong-Hwan Lim, Prof. of Mechatronics. Eng.

Yang Hoi Doh
Yang-Hoi Doh, Professor, Prof. of Electronic Eng.

JEONG DAI JO
Jeong-Dai Jo, Dr., Korea Institute of Machinery and Material

Ki Rin Kwon
Ki-Rin Kwon, Professor, Prof. of Mechanical. Eng.

Kyung Hyun Choi
Kyung-Hyun Choi, Professor, Prof. of Mechatronics. Eng.

February 2017
Date

Department of Mechatronics Engineering
GRADUATE SCHOOL
JEJU NATIONAL UNIVERSITY

I would like to dedicate this thesis to my family, especially to my late mother and my beloved father.

Acknowledgments

In the name of Allah, the most gracious and the most merciful.

First and Foremost, all praise to Allah for giving me this opportunity, and helping me in difficult times throughout my life especially during my PhD. This achievement was not possible without faith in Him, and without His help which kept my heart steadfast and devoted to my research work.

At this juncture my heart is indebted to the sacrifices done by my family, including my late mother, my father, my siblings, my wife and my beloved daughter. All of them were a motivation for me to complete this PhD. Especially my father did a great job at instilling the necessary skills in me, to overcome stress and anxiety due to hard work and taught me how to remain focused, enthusiastic, and motivated during stressful times.

I would like to express my appreciation to my PhD. supervisor, **Professor Kyung Hyun Choi** for his supervision and constant support throughout the programme and during the writing of this thesis. It was an honor to work under his excellent guidance, extreme patience, and constant encouragement during this programme. I would never be able to thank him enough for his moral and financial support in these 4 years of my stay in Jeju Island.

Sincere thanks to all my seniors and mentors at AMM lab including Dr. Khalid Rahman, Dr. Nauman Malik, Dr. Arshad Khan, Dr. Muhammad Naeem Awais, Dr. Maria Mustafa, Dr. Adnan Ali, Dr. Navaneethan Duraisamy, Dr. Sridharan, Jae Hee Park, Dr. Muhammad Zubair, Dr. Murtuza Mehdi, Dr. Kamran Ali, and Dr. Junaid Ali. I am thankful to my lab mates including Ghayas Uddin Siddiqui, Memoon Sajid, Ahmed Kamel, Muhammad Muqeet Rehman, Jahanzeb Gul, Srikanth Jagadeesan, Muhammad Mutee ur Rehman, and Imran Shah. I am thankful to my Korean lab mates including Hyun Woo Dang, Bong Su Yang, Young Jin Yang, Go-Bum Kim,

Hyeon Beom Kim, Soo Wan Kim, Young Soo Kim, Hyotae Kim, and Kyung Hwan Kim for helping me at every step throughout my stay at AMM Lab. I am greatly thankful to all my Pakistani friends particularly Zahid Manzoor, Muhammad Waqar, Rashid Ahmad, Safdar Ali, Farrukh Israr, Ali Shaukat Khan, Sohail Khan, Afaq Muhammad, Zubair Amjad, Waseem Abbas, Gul Hassan, Irshad Ali, and Arshad Hassan.

Finally, I thank the great people of Korea, who are incredibly ambitious, humble and go out of the way to help foreigners like me.

Shahid Aziz, November 2016

Table of Contents

List of Figures

List of Tables

Abstract

Due to an expected increase in the development of wearable devices technology over the next 5 years, the global wearable market demand is likely to increase at a very high rate by 2021. One of the significant factors of wearables is the incorporation of sensors which can monitor people's health and surroundings in real time and continuously. Though the wearable sensors technology appears to be quite attractive and is gradually becoming a necessity in everyday life of common people, this emerging field is imposing several challenges and not much research has been done to address them. One major challenge is to have sensors which can monitor humidity, temperature, motion etc. continuously in real time with ultrafast response and recovery times. Moreover, conventional vacuum based fabrication technologies which are mostly used for the fabrication of sensors, are not very cost efficient, and as a result wearable devices are quite expensive, and out of buying range for most of the people.

This thesis reports on the fabrication and characterization of thin film based printed sensors, which are composed of nano-composite materials. In our research work printed sensors have been fabricated using the cost efficient printed technologies like spin coating, screen printing, D-bar coating, reverse offset printing, and transfer printing on a variety of substrates ranging from glass, PET, and PDMS. All the electrical response characterizations have been done by in-house built characterization setups. The fabrication and quality of printed thin films of nano-composite materials were confirmed by FE-SEM, 3D Nano-Profiler, and optical microscopy. The chemical composition was characterized by X-Ray diffraction (XRD) and Fourier transform infrared spectroscopy (FTIR). Our printed sensors show ultrafast response and recovery time, and cost effective fabrication technologies filling the technological gap in existing fabrication technologies.

Therefore it is believed as a result of current research that nano-composite based thin film printed sensors have a promising future in the emerging field of printed and wearable sensors industry.

Keywords: Thin film, printed sensors, nano-composite, wearable sensors, printed technologies.

1. Introduction

1.1. Importance of Printed Electronics

The term printed electronics can be attributed to a wide variety of electronic thin films, coatings, conductive patterns, and electronic devices that are fabricated on different kind of substrates through various printed technologies. In the recent years, printed electronics has opened up new possibilities in the applications of many devices which include Organic thin film transistors (OTFTs), organic LED (OLED), RFID tags, Memristors, nanogenerators, batteries, stretchable devices, wearable sensors, humidity sensors, temperature sensors, and flex sensors, etc.

Printed electronics has extended its potential applications by providing a wide variety of substrates including glass, silicon, silicon-dioxide, PET, PDMS, textile fabrics, paper, polyimide, animal shell and skin, and plant leaves, etc. This expansion has enabled printed electronics to make a huge contribution in the fields of bio-medical science and technology through bio sensors, disease diagnostic and health monitoring devices. Printed electronics industry is rapidly growing and expanding as a result of active research going on in this field. According to IDTechEx forecast, the market for printed sensors will have increased by more than $1 billion by 2020.

Printing electronics and sensors are attracting increasing interest due to the low cost fabrication and ease in fabrication of large area electronics on flexible and stretchable substrates. Low cost materials, and printing systems are the important factors attracting the keen interest of most researchers in printed electronics.

1.2. Types of printed Sensors

On the basis of sensing, there are many types of sensors. Some of them are classified here.

1.2.1. Humidity sensors

Humidity sensors are the sensors which measure the relative humidity of a particular environment in which they are placed, at a given temperature. Most humidity sensors are resistive or capacitive based on the sensing material used for analyzing the humidity levels in the environment. Humidity sensors are mostly used in food industries, environment monitoring, and breathe monitoring applications.

1.2.2. Temperature sensors

Temperature sensors are the sensors which measure the temperature changes of a particular environment. Temperature sensors are mostly resistive based sensors, which change their resistance with the change in temperatures. Temperature sensors vary from simple ON/OFF thermostatic devices which control a domestic hot water heating system to highly sensitive semiconductor types that can control complex process control furnace plants.

There are many different types of temperature sensor available and each type has different characteristics depending upon their actual application. A temperature sensor consists of two basic physical types:

- Contact temperature sensor- These types of temperature sensor are required to be in physical contact with the object being sensed and use conduction to monitor changes in temperature. They can be used to detect solids, liquids or gases over a wide range in temperatures.

- Non-contact temperature sensor- These types of temperature sensor use convection and radiation to monitor changes in temperature. They can be used to detect liquids and gases that emit radiant energy as heat rises and cold settles to the bottom in convection currents or detect the radiant energy being transmitted from an object in the form of infra-red radiation (the sun).

1.2.3. Pressure sensors

Pressure sensor is required to detect the pressure and/or its change, and to convert it accurately and repeatedly into an electrical signal utilizing a physical operating principle. The electrical signal is then a measure of the magnitude of the applied pressure or change in pressure. Most common type of electrical signal based pressure sensors are resistive pressure sensors, piezo-resistive pressure sensors, capacitive pressure sensors, and piezo-electric pressure sensors depending upon the type of response shown by the sensing material of the sensor.

1.2.4. Strain/Flex sensors

Flex sensors are simpler form of strain sensors that can only measure bending in contrast to strain sensors that are also able to measure elongation or strain in addition to bending. This simplicity makes the flex sensors easier and cheaper to fabricate as compared to strain sensors. The working principle of flex sensors is based on the change in resistance of the active film upon bending angles relative to its straight position.

1.2.5. Biosensors

A biosensor is an analytical device which converts a biological response of a specific biological recognition element into an electrical signal. Since its inception, biosensors have been expected

to play a significant analytical role in medicine, agriculture, food safety, homeland security, environmental and industrial monitoring.

1.2.6. Light sensors/ Photo sensors

Light sensors creates an output signal indication the intensity of light by measuring the radiant energy that exists in a very narrow range of frequencies called light. It converts the light energy into an electrical signal output. They are also known as photoelectric devices or photo sensors as photons are converted to electrons. Light sensors can be divided into two categories based on output.one sensor which converts light energy to electrical energy and those which change their electrical properties in some way such as photo-resistors or conductors. Photoelectric sensor has basically 5 components, light source, light detector, lenses, logic circuit and output.

1.2.7. Gas sensors

Gas sensor is a device that detects the presence of gases in an area. Gas sensors can be used to detect combustible, flammable and toxic gases and oxygen depletion. A chemical sensor comprises of a transducer and an active layer for converting the chemical information into another form of electronic signal like frequency change, current change or voltage change. Gas detectors can be classified according to the operation mechanism (semiconductors, oxidation, catalytic, photoionization, infrared, etc.)

1.3. Fabrication Technologies for Printed sensors

In the recent years printing technology has been widely used for the fabrication of sensors. Printed sensors have an added advantage of patterning conductive and functional inks onto various substrates layer by layer, which enables the sensors to be built more directly and continuously as

contrary to the traditional silicon based semiconductor industry. Several technologies which have the potential to be used for printing sensors are reviewed in this section.

1.3.1. Spin Coating

Spin coating is one of the most common coating techniques used to deposit uniform thin films onto a wide variety of flat substrates. Spin coating is performed by rotating the substrate and pour the ink on it. The excess ink is flug off the side under the effect of centrifugal forces. Air pressure is used along with centrifugal forces for ultra-thin films. The spin coating has limitations such as it is limited to small areas, material significant and this technique cannot be adopted for mass scale production.

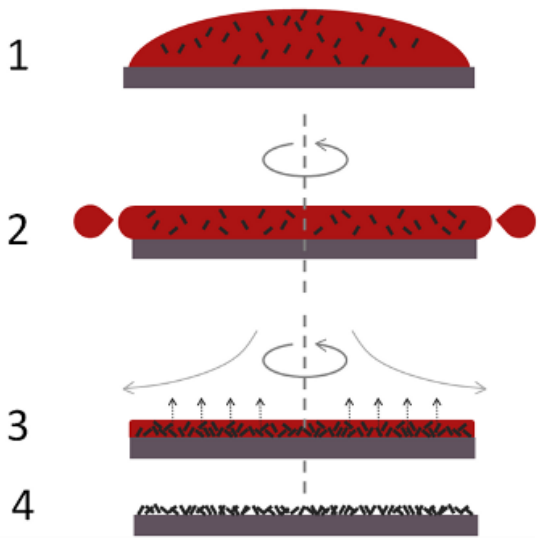

Figure 1-1: Example of spin coating using a static dispense

1.3.2. D-bar coating

Figure 1-2 shows the system photograph in which a D-bar roller rolls over the substrate surface and the thickness is controlled by the gap between the steel bar and the substrate. Once the substrate is placed on the platform, vacuum is turned on from the touch control panel to hold the substrate

firmly and avoid slipping while the rod is rolling on the substrate. Then the rod is moved to a suitable position and height by manually adjusting the control knobs, which increase or decrease the rod height above the substrate by applying a pressure through springs as shown in inset of Figure 1-2. Ink is then poured on the steel bar, and the bar is rolled on its axis, while not touching the substrate to fully spread the ink on its surface. Once the bar is covered with ink, it is then slowly rolled on the substrate surface. The rolling speed and linear speed of the bar is controlled from the control panel.

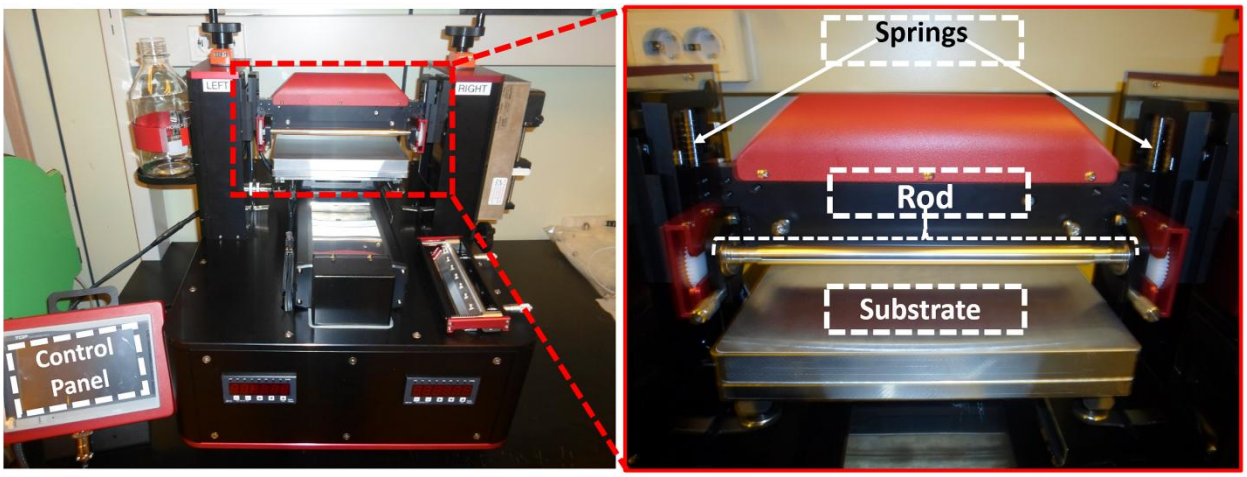

Figure 1-2 D-bar coating system for coating thin films

1.3.3. Screen printing

Screen printing technology offers an appealing way to design new generation of sensors. Screen printed electrodes have been utilized as a tool to design disposable and portable sensors for environmental monitoring. In screen printing a woven mesh is used to transfer ink from the open areas of the mesh while restricting ink flow from the rest. A high viscosity ink is used in screen-printing which is squeezed through the screen via a squeegee. During deposition, the substrate is placed just around a mm below the screen, and is hold in place via a vacuum pump. The thickness

of the printed pattern depends on the screen thread diameter, mesh count and viscosity of the ink. The working procedure of screen-printing system is shown in Figure 1-3.

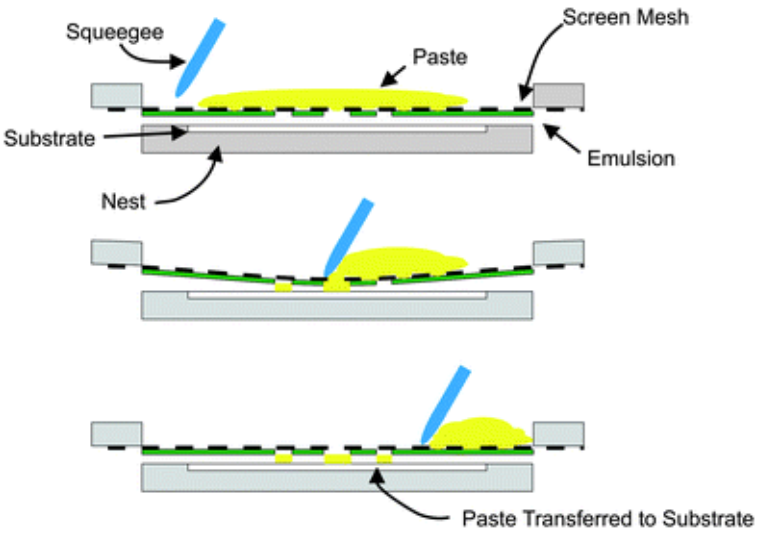

Figure 1-3: Screen printing process

1.3.4. Slot die printing

Slot die is a very simple method of coating, which is used for high volume printing. Slot die is an ink dispensing system that has three main components, which are cavity body, ink pump and die. The ink pump infuses the ink into the cavity and ink is forced out of cavity from the die lips. The lips of die are in close proximity above the substrate that moves at a uniform speed via roll-to-roll process. The parameters which control the deposition thickness are web tension, velocity, flow rate and the gap between the die lips and substrate. Figure 1-4 shows the slot die system.

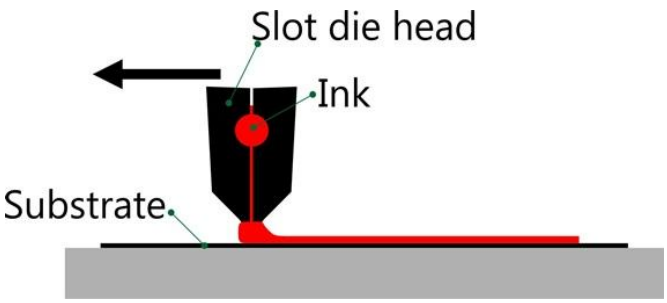

Figure 1-4: Slot Die process schematic

1.3.5. Inkjet printing

Inkjet printing is a non-contact printing process in which a pattern can be printed directly onto a substrate through a nozzle. The printing is controlled by a computer programme and image on the computer can be printed on the substrate without any intermediate plate, roll or screen. This makes printing process quite flexible as compared to the conventional processes. Figure 1-5 shows the inkjet printing process.

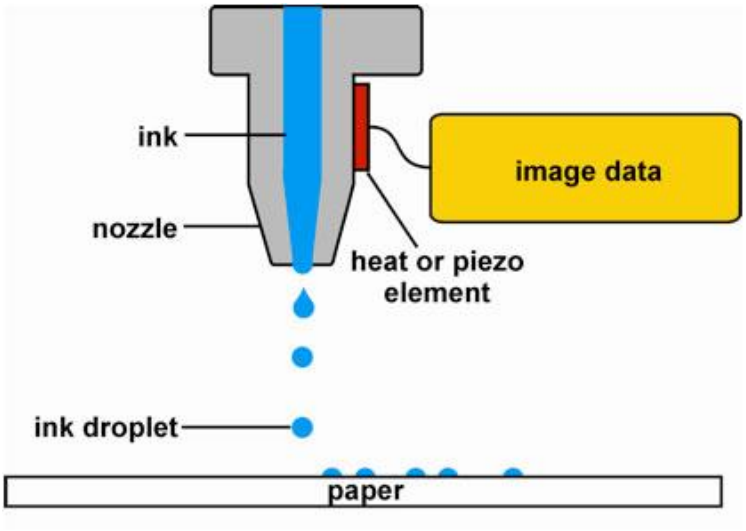

Figure 1-5: Inkjet printing process schematic

1.3.6. Electrohydrodynamic printing

Electrohydrodynamic (EHD) printing is a well-established direct printing technique for micro/nano-scale fabrication to achieve highly sensitive electronic devices. While most electronic devices are manufactured by conventional lithographic methods, the development of a cost-effective and non-conventional approach to print fine resolution conductive patterns is a much desired goal in the printed electronic community. The key advantage of using EHD printing over conventional printing techniques is the ease of printing fine resolution patterns and ejecting high viscosity inks. In order to overcome the limitations of high fabrication cost, complicated equipment

and time consumption, EHD printing have attracted increasing attention in the printed electronics industry for the last decade. EHD is performed under ambient temperature and pressure conditions and more throughput and speed than other inkjet techniques. EHD printing is useful in many applications including sensors. EHD can be performed in continuous and drop-on-demand (DOD) modes. In continuous mode printing is performed after a stable Taylor-cone jet of ink is achieved at the tip of the nozzle, while in DOD patterns are created by falling droplets at certain frequency over a suitable substrate. The lines can be created by controlling the speed of the nozzle head, and the frequency of the ejecting droplets in DOD. A simple EHD printing set up is shown in the Figure 1-6.

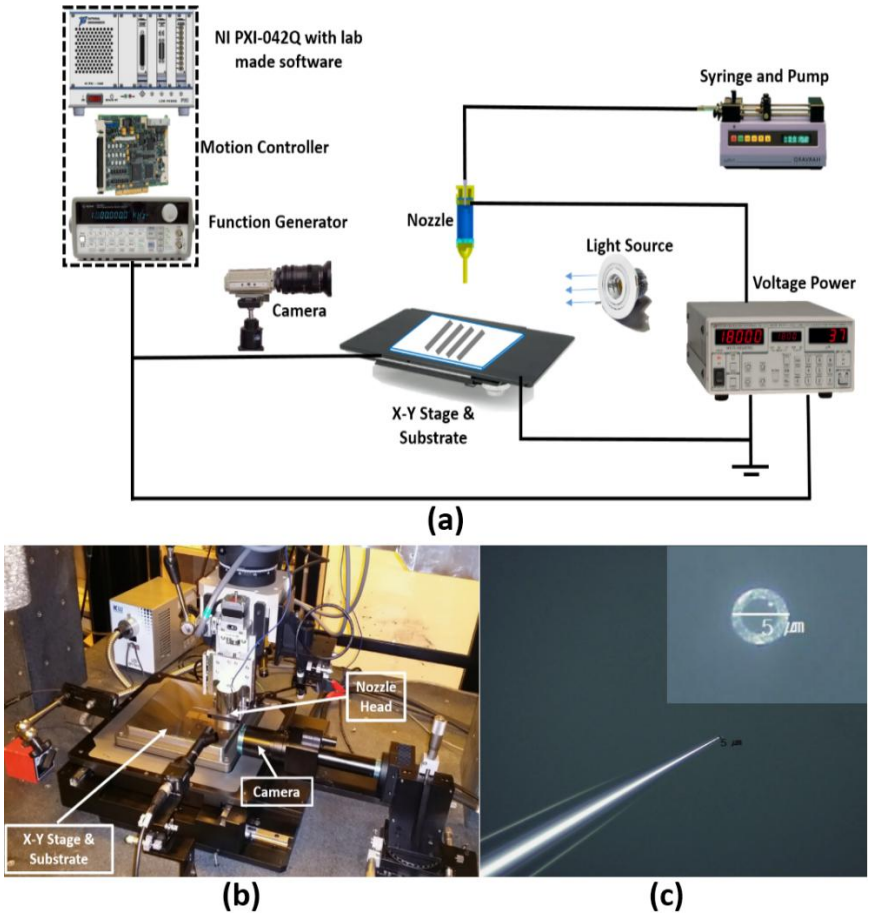

Figure 1-6: (a) Schematic of EHD drop on demand printing system (b) Photograph of the real EHD printing system used for printing micro patterns (c) Microscope image of the micro-nozzle, inset showing the top view and outer diameter of the nozzle tip.

2. Fabrication of Environmental Sensors

2.1. Humidity Sensor Based on PEDOT: PSS and Zinc Stannate Nano-composite

A composite of PEDOT:PSS and zinc stannate (ZnSnO3) has been introduced for impedance based humidity sensing, owing to its high sensitivity, good stability, very fast response (~0.2 s) and recovery time (~0.2 s), small hysteresis, repeatability, low cost fabrication and wide range of sensitivity. Both materials were mixed in three different weight % ratios, to optimize the performance of the sensors. Best response was observed for 5 wt% PEDOT:PSS and 5 wt% ZnSnO3. The impedance of the sensor was dropped immensely from 1.5MΩ to 50kΩ by changing relative humidity from 0-90%. The reason for this improvement in sensitivity was analyzed by virtue of sensing mechanism and different characterizations (3D nano profiler, optical microscope, and FTIR spectroscopy) revealing the surface morphology and chemical structure of the film. Due to its response and ability to sense human breath and skin humidity, it is suitable for environment, artificial skin and food industry applications.

2.1.1. Introduction

Relative humidity (RH) is defined as the ratio of the partial pressure of water vapors in air to the saturation vapor pressure of the air at a given temperature. Relative Humidity sensors have been fabricated extensively using conductive polymers[1–3], polymer-metal oxide composite[4], semi conductive materials[5], nano-composites of polymers with nano-rods[6,7] and nano-wires etc. PEDOT:PSS[8] and pure $ZnSnO_3$ have been used alone in many sensors including humidity sensors. $ZnSnO_3$ has been used in the sensing of Ethanol[9], H_2[10], H_2S, HCHO, C_2H_5OH[11], and humidity sensing[5][12][13]. On the other hand PEDOT: PSS has also been widely used for sensing of gases[14][15], as well as for humidity sensing.

Polymer based humidity sensors have been widely studied in research and applied in industry for more than 30 years. Among polymer materials, PEDOT:PSS has been used extensively for humidity sensing, because of its increased conductivity and resistive response to humidity changes. PEDOT:PSS inkjet printed on quartz crystal microbalance has been utilized for humidity sensing[8], but the response time is slow. In a similar work, PEDOT:PSS has been inkjet printed on piezoelectric cantilever[16] for resistive based humidity sensing, but the response time is slow as well and the humidity measurement range is limited (20.28 to 66.29%RH). A resistivity based PEDOT:PSS humidity sensor[17] was analyzed for humidity sensing below 80%RH. To enhance the sensitivity of PEDOT:PSS, nanoparticles like SiO_2 and aluminum zinc oxide (AZO) have been introduced into the polymer to form nano-composites[18], but the limitation of linear response range (20 to 60%RH) remains an issue which needs to be resolved. The response time of PEDOT:PSS based humidity sensor was highly improved (~1s) by adding iron oxide nanoparticles[4], keeping the humidity sensing range for linear response still limited to (30-70%RH). A low power CMOS based AZO/PEDOT:PSS sensor[19] has been used for humidity sensing (0-75%RH), but the resistance of the sensing layer is doubled within 40 days because of the change in the structure of PEDOT:PSS chains by the absorption of moisture and oxygen.

Nokia research center based in United Kingdom has developed humidity sensors from 2D GO (graphene oxide), which showed ultrafast response (~30ms) for humidity change within (30 – 80% RH) range[20]. A wide range (0-97% RH) humidity sensor was developed from Poly(4-vinylpyridine)/carbon black composite which showed linear resistive response, eliminating the issue of low humidity detection using resistance based polymeric humidity sensors[21][22]. Ultrafast humidity sensor for breath monitoring has been recently developed by using coronene tetracarboxylate and dodecyl methyl viologen supramolecular nanofiber[6].

On the other hand, there is a wide class of ceramic materials, which have been used for humidity sensing on a large scale for the last decade. Among ceramic materials, $ZnSnO_3$ nano structures have been used for resistive based humidity sensing[5] with a wide range of sensing (0-90%RH), but the results were reproducible up to ±77% of the previous value after two months. Zinc stannate (Zn_2SnO_4) thin films have been used by T.Donchev et.al [12] to sense relative humidity with response and recovery times upto several minutes. Thin films of cubic structured $ZnSnO_3$ [23] were deposited with different immersion times to investigate the humidity sensing properties of the films. The response time was in several seconds and the humidity sensing range was limited to (40-90% RH). An organic-inorganic composite based on (PEPC+NiPc+Cu_2O) was analyzed by Zubair Ahmed et.al[24] for humidity sensing, which showed capacitive humidity response for humidity levels ranging from (40-100%), with response and recovery times of ~10 s.

Although great efforts have been done by various groups to improve the performance of relative humidity sensors using different combinations of ceramic and polymer materials, but they have experienced great challenges achieving fast response along with wide range humidity sensors. A detailed comparison of humidity sensors fabricated from different materials has been done in our previous work[25].

In this work, $ZnSnO_3$ nanostructures were introduced into PEDOT:PSS matrix for study of relative humidity sensing. The two materials were mixed in different ratios by weight percentage to optimize the performance of the sensor. Adding $ZnSnO_3$ has greatly improved the humidity sensing range as well as the response and recovery time of the fabricated humidity sensor as compared to the previously reported ones. It has been proved that the new proposed material nano-composite is a good candidate for the humidity sensing materials.

2.1.2. Experimental

Synthesis of materials

Zinc stannate ($ZnSnO_3$) in cubic crystallites form was prepared from zinc sulphate heptahydrate ($ZnSO_4.7H_2O$) and sodium stannate trihydrate ($Na_2SnO_3.3H_2O$) precursors by hydrothermal process as reported by[26]. The used Poly (3, 4-ethylenedioxythiophene) Polystyrene Sulfonate or (PEDOT:PSS) was Orgacon EL-P5010 solvent based paste with 3 wt% solid content. The materials utilized for the fabrication of nanocomposite sensing film are relatively impure and commercially used as dyes, owing to the low cost of the sensor fabrication.

PEDOT:PSS was prepared by dissolving 5 wt% PEDOT:PSS paste in IPA(Isopropyl alcohol, C_3H_8 , purity $\geq$ 99.5%). After shaking vigorously, the solution was bath sonicated for 10 minutes, and stirred with a magnetic stirrer for 2 hours at 1000 rpm and 30°C.

The mixtures were then bath sonicated for 30 minutes, and magnetically stirred for 4 hours to obtain the nano-composite dispersion of PEDOT:PSS and $ZnSnO_3$ for three different weight percentages. The inks were then ready to be used for sensors fabrication.

The structures of $ZnSnO_3$ and PEDOT:PSS are shown in Figure 2-1-1(a) and (b).

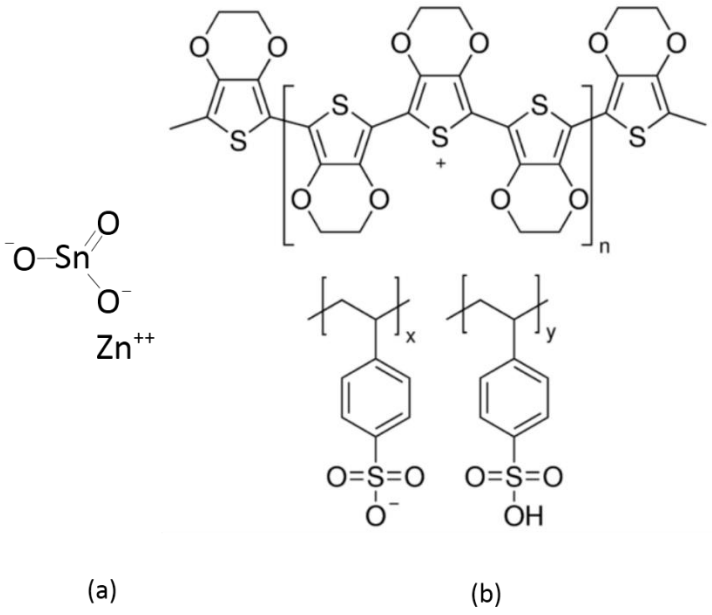

Figure 2-1-1: Structural formulae of (a)$ZnSnO_3$ and (b)PEDOT:PSS[27]

In metal oxide humidity sensors, H_2O is adsorbed on the oxide surface in molecular and hydroxyl forms. Water molecules increase the conductivity of n-type ceramics and decrease the conductivity of p-type ceramics[28]. This effect has been attributed to the donation of electrons from the chemically adsorbed water molecules to the ceramic surface. Water molecules replace the previously adsorbed and ionized oxygen (O^-, O^{2-}, etc.) and therefore release the electrons from the ionized oxygen. The water layer formed by the physical adsorption may be somewhat proton-conductive. Therefore, at room temperatures the conductivity of ceramic semiconducting materials is actually due to addition of both electrons and protons (ionic)[29]. On the other hand organic polymers are macromolecules in which a unit structure repeats. Most of the polymers are carbon-hydride compounds or their derivatives. The film is filled with micro-pores for water vapor condensation and some of the measurable physical properties change due to the water absorption.

Sensor Fabrication

Sensor structure consists of 20 pairs of gold interdigitated electrodes (IDTs) fabricated by photolithography on a piezoelectric $LiNbO_3$ substrate. The distance between two consecutive electrode fingers and the width of each electrode is 50µm each as shown in Figure 2(b). The sensing layer of nano-composite material was deposited on the IDTs using ACE-200 spin coater at 1200 rpm for 30s. The fabricated sensors were then allowed to dry in oven (SciLab^{TM} SOF Ovens Forced Convection-type) at 120°C for 3 hours. The as-fabricated sensor is shown in Figure 2-1-2(a).

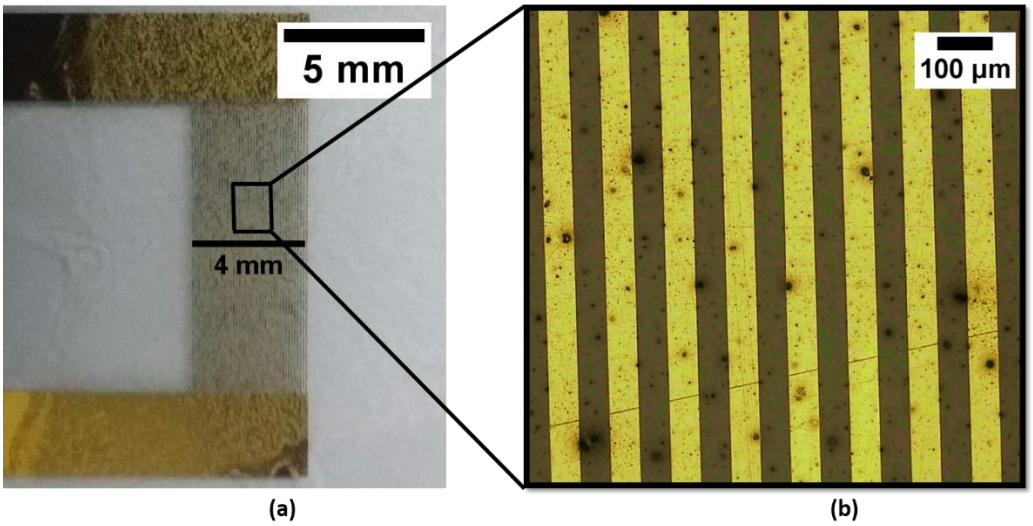

Figure 2-1-2: Fabricated sensor optical image (a) Zoomed (microscopic image (10X)) showing IDTs dimensions (b)

Characterization of sensing layer

The film was characterized optically (optical microscope, 3D nano profile Ellipsometry, and FESEM), as well as chemically (FTIR spectrum) to ensure the film thickness, surface morphology, and chemical bonding in the nano-composite materials. The microscopic images in Figure 3(a,b,

and c) show the surface of sensing layer fabricated on IDTs at different resolutions. Figure 2-1-3(a) shows the contrast between the bare glass surface and film surface, showing the fully covered glass surface by the nano-composite film. Figure 2-1-3(b) shows the IDTs surface covered with the sensitive material, also it shows the dimension of the IDTs, and Figure 2-1-3(c) is a zoomed in microscopic view at 100X resolution of the sensitive material on the substrate surface. From Figure 2-1-3 it can be visually observed that the overall film of the nanocomposite contains PEDOT:PSS (black spots) and the blend is uniformly spin coated on the IDTs and the substrate.

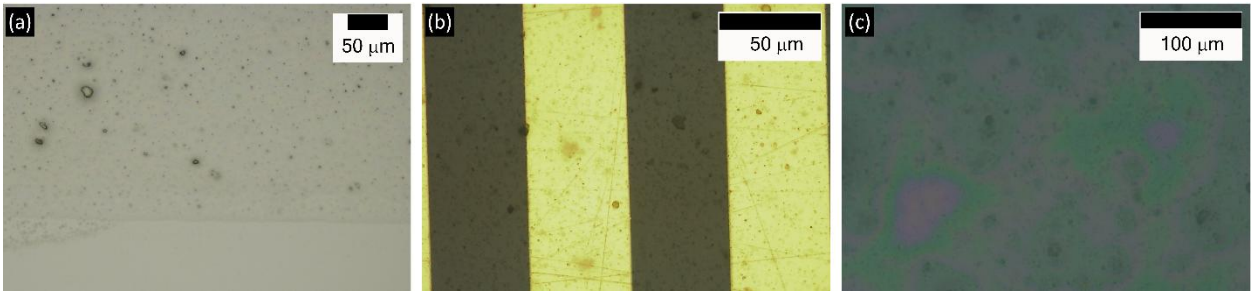

Figure 2-1-3: Microscopic images of the $ZnSnO_3$and PEDOT:PSS nano-composite sensing layer at 20X (a), 50X on IDTs (b), and 100X (c) resolutions. Scale bar is 50μm in each case.

The 3D Nano profiles of the films surfaces were obtained by NanoView high accuracy non- contact surface profiler and are shown in Figure 2-1-4 (a,b,&c). Figure 2-1-4(a and b) show the surface profiles of the neat $ZnSnO_3$ and PEDOT:PSS films surface.

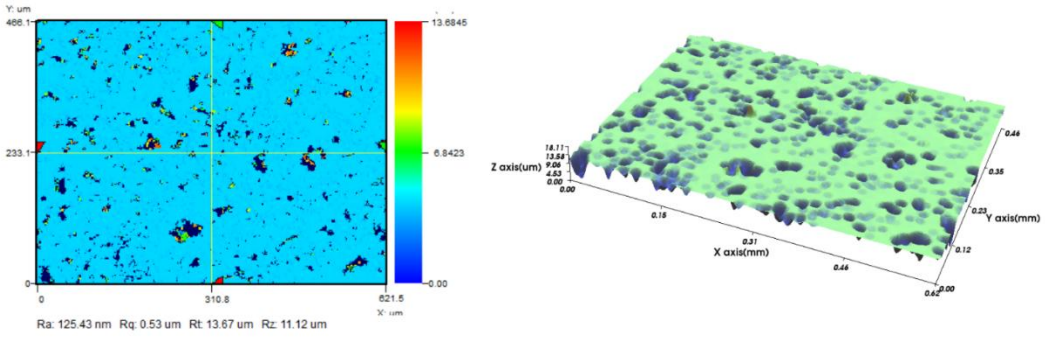

Figure 2-1-4(a): Noncontact 3D surface profiler images of neat $ZnSNO_3$ showing the highly porous nature of the film.

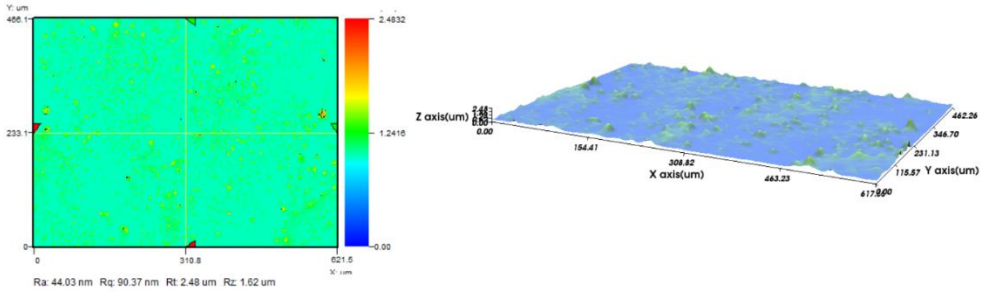

Figure 2-1-4(b): Noncontact 3D surface profiler images of neat PEDOT:PSS showing the solid content in the film.

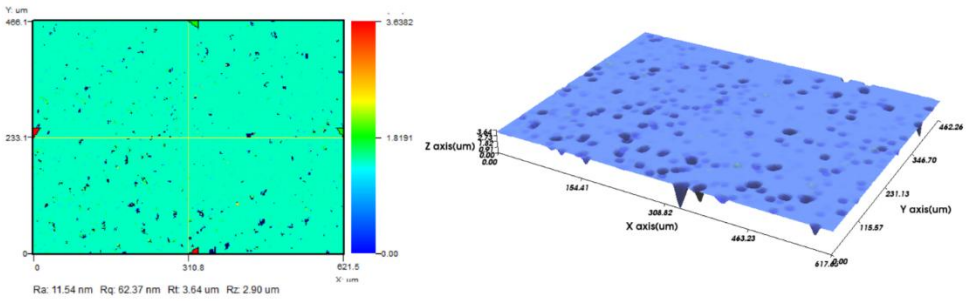

Figure 2-1-4(c): Noncontact surface profiler images of the (PEDOT:PSS + $ZnSnO_3$) nanocomposite sensing layer film.

Figure 2-1-4(c) shows the surface profiles of PEDOT:PSS and $ZnSnO_3$ nanocomposite spin coated at the same parameters as the neat PEDOT:PSs and $ZnSnO_3$ films. It can be seen clearly that neat PEDOT:PSS is less porous as compared to $ZnSnO_3$ and by adding zinc stannate into the PEDOT:PSS matrix, the resulting film has increased porosity as compared to neat PEDOT:PSS but less than the cubic $ZnSnO_3$ film The $ZnSnO_3$ cubic crystallites grown by hydrothermal process have a lot of pores in the film as shown in the FESEM image in the Figure 3 in our recent manuscript[26]. In Figure 2-1-4(a) the dark blue spots in the 3D profile indicate the pores in the $ZnSnO_3$ film. Pure PEDOT:PSS shows almost no pores in thin film, and hence by addition of $ZnSnO_3$ in PEDOT:PSS the porosity (dark blue holes) of the film has considerably increased as shown in Figure 2-1-4(c). The increased porosity plays a great role in the response time and linearity of the impedance vs humidity curves, and will be discussed in the results and discussion section.

The thickness of the fabricated nano-composite film was around 400nm as measured by state-of-the-art, nondestructive, Ellipsometry system (K-MAC Spectra Thick Model: ST4000-DLXn). The film thickness was also confirmed through cross sectional analysis of thin film using FESEM (JEOL JSM- 7600F, Japan). The value of film thickness as obtained from FESEM was ~ 410 nm which is approximately equal to the thickness measured by the Ellipsometry system.

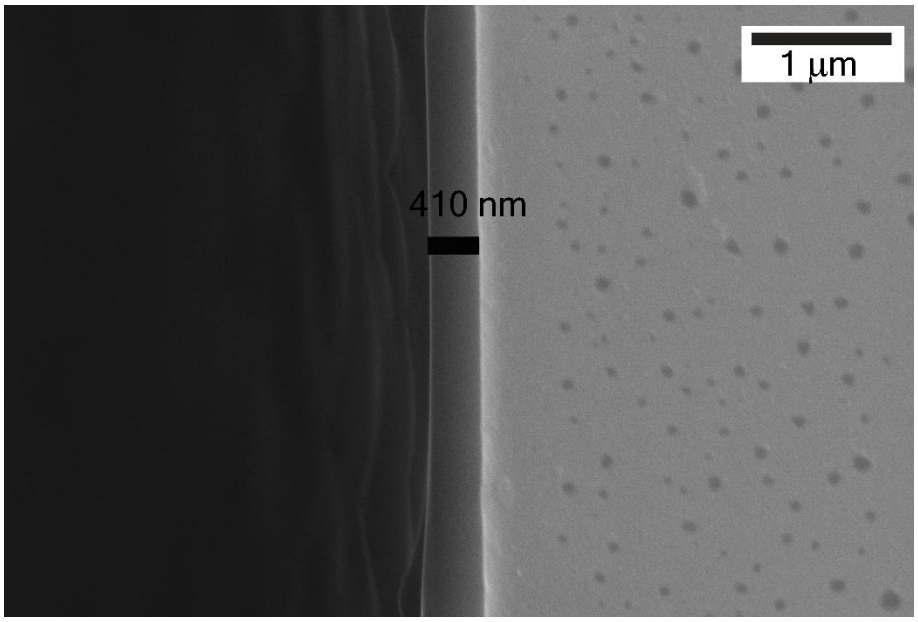

Figure 2-1-5: Cross-Section FESEM image of $ZnSnO_3$ and PEDOT:PSS nano composite film on $LiNbO_3$ substrate.

The Fourier transform infrared radiation (FTIR) analysis of the film was carried out to reveal the chemical and elemental footmarks of $ZnSnO_3$ and PEDOT:PSS in the nano-composite film.

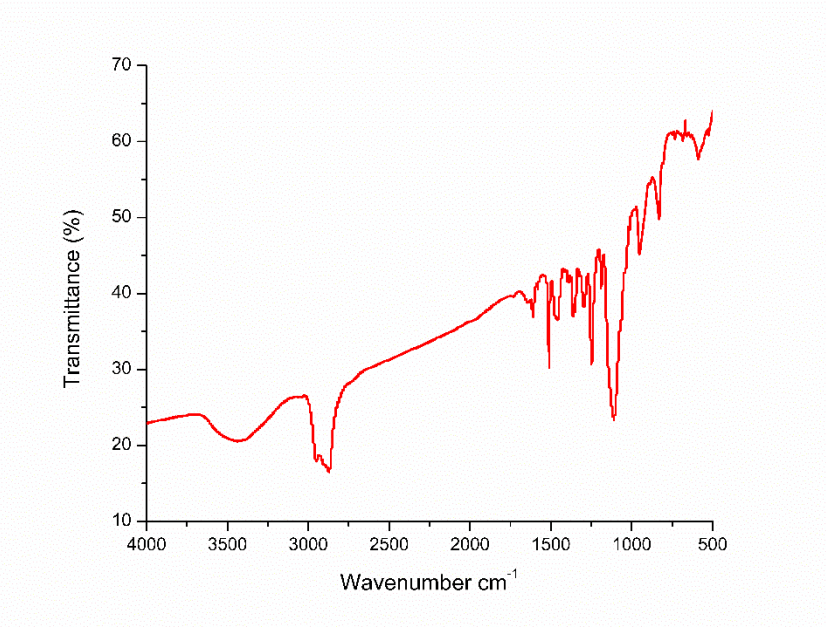

Figure 2-1-6: FTIR spectrum for the PEDOT: PSS and $ZnSnO_3$ nano-composite sensing layer.

In the FTIR spectrum shown in Figure 6, the bands observed at 540, 587, and 1110 cm^{-1} are attributed to the presence of M-O or M-O-M groups which are characteristic of $ZnSnO_3$[30]. The bands at 830 and 949 cm^{-1} represent the vibrations of S–C bonds in polymerized PEDOT chain[31]. The band at 1180 cm^{-1} is assigned to the stretching of the C−O−C bonds in the ethylene dioxy group[31]. The bands at 1250, 1360, 1460, and 1510 cm^{-1} correspond to the stretching of thiophene ring[32]. The occurrence of bands at 2870 and 2950 cm^{-1} account for alkyl C−H stretching vibrations[33]. The bands at 1640cm^{-1} and 3430 cm^{-1} are attributed to the bending and stretching vibrations of the O-H group[33].

2.1.3. Measurement of humidity sensing response

Humidity sensing response of the sensor was studied in a custom made humidity chamber. The setup and working mechanism of the humidity chamber is shown in Figure 2-1-7. The sample sensor to be analyzed was placed alongside the reference sensor inside the humidity chamber. The reference sensor used in this setup was HTU21 temperature and humidity sensor, which is capable

of measuring humidity to the accuracy of ±2% RH and a resolution of 0.04% RH. The response time of the reference sensor is <5s and the temperature coefficient is -0.15%RH/°C. The sample sensor was connected to the digital LCR meter (Applent AT825) to give the feedback of impedance and time to the computer via a USB datalogger. The reference sensor was also connected through an interface circuit to the computer giving the real time values of relative humidity and time inside the humidity chamber.

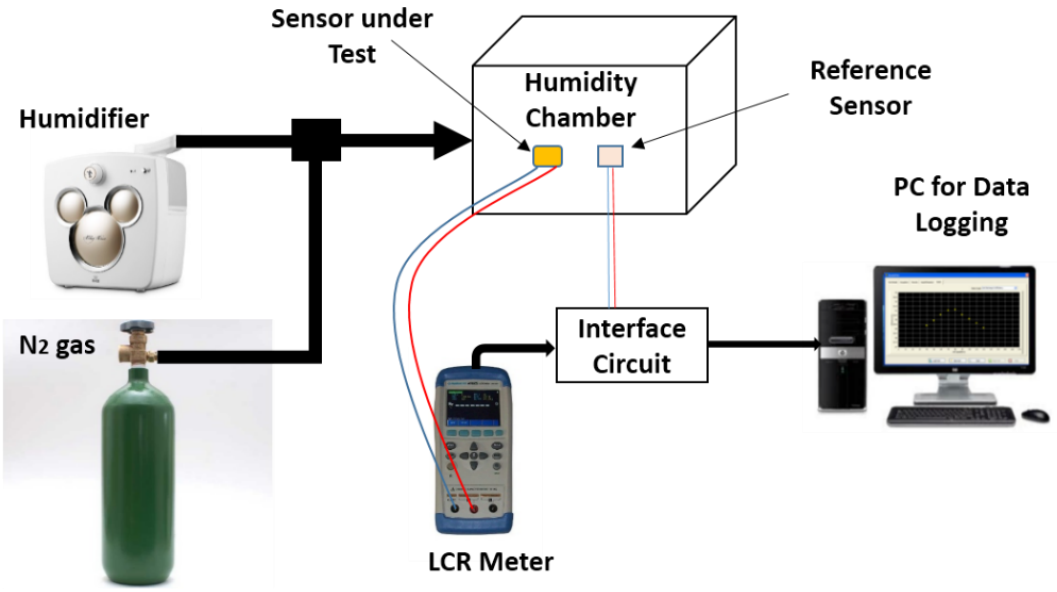

Figure 2-1-7: Humidity Chamber setup showing the airflow direction, two sensors in the humidity chamber, and data logging from digital LCR meter to PC via USB interface circuit.

After setting up all the connections, humidity was introduced into the humidity chamber via ZENUS humidifier and the data was logged per second for increasing humidity level until the relative humidity reached 90%, after which the humidity supply was cut off and dry nitrogen gas was introduced imperceptibly into the humidity chamber from a separate inlet to decrease humidity back to 0%. The same procedure was repeated to get the response of the sensor for the whole range of absorption and desorption of the humidity and to see the hysteresis effect in the sensor response. One complete cycle of adsorption and desorption took approximately 20 minutes.

2.1.4. Results and discussion

The sensor response to humidity adsorption and desorption from (0-90% RH) at 1kHz test frequency for different concentrations of PEDOT:PSS and $ZnSnO_3$ in the nano-composite is shown in Figure 2-1-8(a,b and c). The Figure 8 shows the effect of changing concentrations of PEDOT:PSS and $ZnSnO_3$ on the sensor response in the form of impedance change.

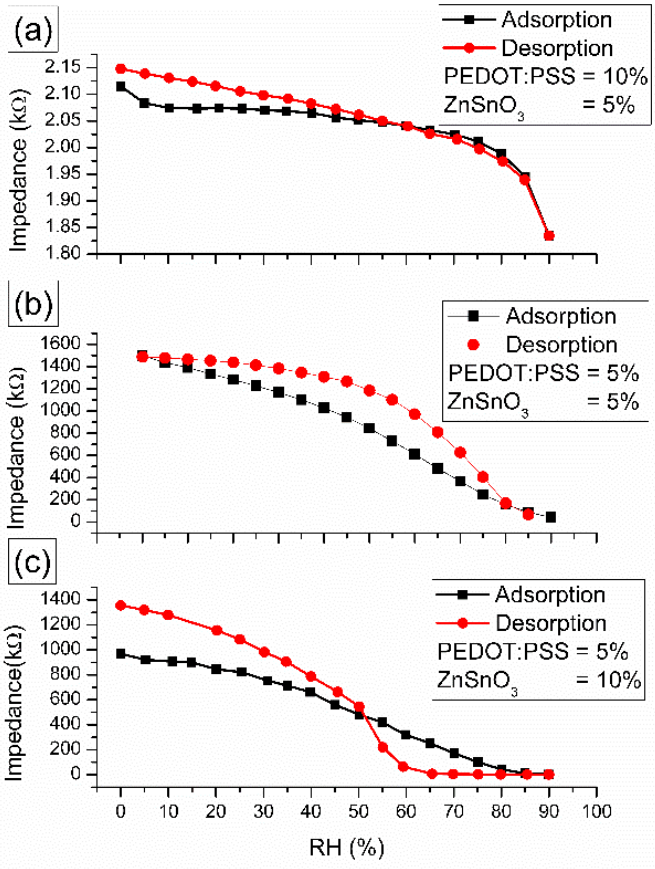

Figure 2-1-8: Impedance vs RH adsorption and desorption curves of PEDOT:PSS and $ZnSnO_3$ nano-composite at different weight concentrations of PEDOT:PSS and $ZnSnO_3$. (a) PEDOT:PSS 10% and $ZnSnO_3$ 5% (b) PEDOT:PSS 5% and $ZnSnO_3$ 5% (c) PEDOT:PSS 5% and $ZnSnO_3$ 10%

The Figure 2-1-8(a) shows that when the concentration of PEDOT:PSS is twice as compared to that of $ZnSnO_3$, the range of impedance is very small (1.84 kΩ to 2.15 kΩ). This behavior is due to the small number of pores in the film, because amount of PEDOT:PSS is high in the composite. The Figure 8(b) indicates that while increasing humidity from 0 to 90% RH, the impedance of the

sensor decreased from ~ 1.5MΩ to ~ 50kΩ. This wide range of sensitivity is attributed to the cubic crystallite structure of $ZnSnO_3$ which increases the surface area and porosity of the sensing film. The effect of increasing the concentration of $ZnSnO_3$ to twice that of PEDOT:PSS in the nano-composite is shown in Figure 2-1-8(c). By increasing the $ZnSnO_3$ concentration in the nano-composite after a certain weight percentage, the desorption process is delayed, as the water molecules get trapped into the pores generated by the cubic structures of $ZnSnO_3$ (as shown in Figure 2-1-4(a)), hence increasing the hysteresis. As the water molecules are trapped in the pores of the film, if the number of pores are more, then it takes more time to decrease humidity from the sensor film, hence the impedance change is very low from the humidity decrease in the range (90% to 60% RH). Once the humidity level reaches 60%, the sensor starts giving response close to linear. Therefore the best performance shown by the sensor was at equal percentages of PEDOT:PSS and $ZnSnO_3$ in the nano-composite. The impedance curves shown in figure 8 are averaged for five consecutive runs from (0-90%) humidity adsorption and desorption.

The response time (10-90% of the maximum value) and recovery time (90-10% of the maximum value) of the sensor is shown in Figure 2-1-9. The response and recovery time shown in Figure 2-1-9(b) are actually the values taken from one cycle of adsorption and desorption cycles shown in Figure 2-1-9(a). It can be clearly observed that by adding $ZnSnO_3$ the response and recovery time of the sensor has been decreased to a great extent, as compared to pure PEDOT:PSS, and pure $ZnSnO_3$.

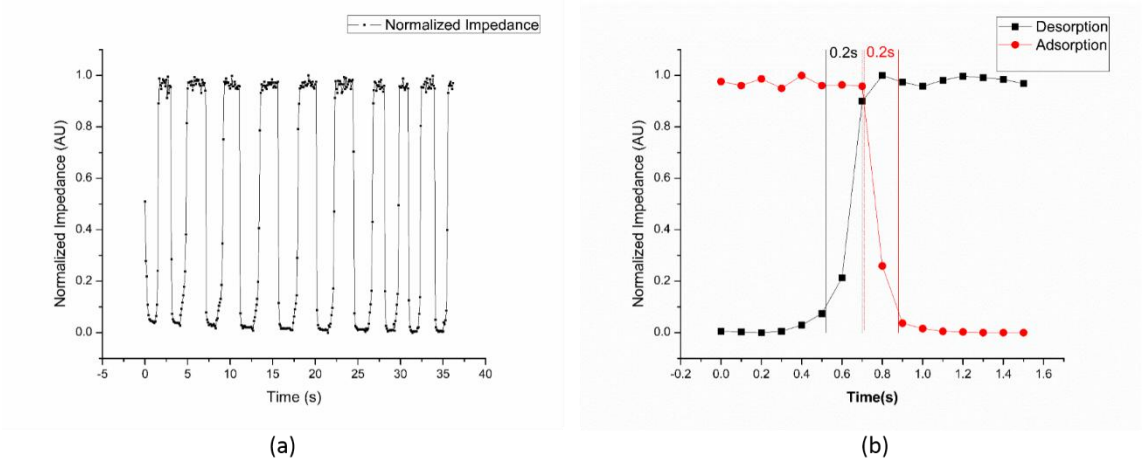

Figure 2-1-9: (a) Normalized response and recovery time of the fabricated sensor (b) Normalized response and recovery time for one cycle (zoomed in version of (a).

It can be seen in the figure that the response and recovery time of the sensor fabricated from nano-composite of PEDOT:PSS and $ZnSnO_3$, is quite fast when compared to the previously reported humidity sensors. This fast response can be attributed to the fact that a piezoelectric substrate has been incorporated in the fabrication of IDTs. In our case the piezoelectric substrate is $LiNbO_3$. When the IDTs are supplied with a high frequency, Surface Acoustic Waves (SAW) are generated within the piezoelectric substrate[34], which help the water molecules to escape easily and readily from the film material. This phenomenon minimizes the saturation of the film surface with water molecules, which is highly responsible for the slow response and recovery times in the previously reported humidity sensors.

2.1.5. Hierarchical Comparison

Based on the characterizations, results, and discussions, a hierarchical table has been formulated presenting the comparison of different formulations of the conductive polymer-metal oxide composite presented in this research work and the previously carried out research works using different types of composite materials for humidity sensing. The detailed comparison presented in Table 2.1 shows that the unique structure of the sensor incorporating SAW effect in a novel

approach with a conductive polymer- metal oxide composite as sensing layer significantly improves the performance of the sensor in terms of measureable range, sensitivity, response time, recovery time, reliability, stability, and accuracy of the sensor output.

Table 2.1: Comparison of current research work with previous literature proving the superiority and novelty

Materials	**Composite Type**	**Sensor Structure**	**Phenomenon**	**Sensing Range**	**Sensitivity**	**Response Time**	**Recovery Time**	**Output Error**	**Reference**
n-BA + DAEMA	Cross linked Copolymer	Simple IDT	Resistive	20-95 %RH	66 kΩ/%RH	~55 seconds	~55 seconds	± 2.0%	[35]
CB-PVP	Conductor-Polymer	Simple IDT	Resistive	10-100 %RH	10 Ω/%RH	Not Measured	Not Measured	Not Reported	[22]
MWCNT + Polyimide	Conductor-Polymer	Bi-Electrode Structure	Resistive	10-95 %RH	2.8 Ω/%RH	Not Measured	Not Measured	~1 %	[36]
Cellulose + Polypyrole	Polymer-Polymer	HF IDT	Capacitive	30-90 %RH	0.09 pF/%RH	~418 seconds	~418 seconds	~1 %	[37]
PAni + PVA	Polymer-Polymer	Comb Shaped	Conductivity based	**5-100 %RH**	100 Ω^{-1}/%RH	~45 seconds	~540 seconds	Very High	[38]
AgNP's + PVA	Metal-Polymer	Differential IDT	Voltage Difference	10-60 %RH	6 mV/%RH	~10 seconds	~10 seconds	Quite High	[39]
NaOH+NaCl+PVA+PEG	Salt-Base-Polymer	Ring Electrodes	Resistive	30-70 %RH	37 kΩ/%RH	Not Measured	Not Measured	Very High	[40]
Quaternized-4VP-c-BuMA	Polymer Electrolyte	Simple IDT	Impedance based	33-95 %RH	161 Ω/%RH	~13 seconds	~13 seconds	~1 %	[41]
Quaternized Polypyrole	Conductive Polymer	Simple IDT	Impedance Based	10-95 %RH	0.037 (slope)	41 seconds	120 seconds	~1 %	[3]
Poly-Aniline	Conductive Polymer	FET Based	Impedance Based	36-90 %RH	**15 MΩ/%RH**	~8 seconds	~27 seconds	Not Reported	[42]
PEDOT:PSS	Conductive Polymer	Micro-Cantilever	Piezo-Resistive	20-66 %RH	4.3 mΩ/%RH	Not Measured	Not Measured	>2.3 %	[16]
Polyamide + PEDOT:PSS	Polymer-Polymer	Fibers b/w Cu-plates	Resistive	25-95 %RH	350 Ω.cm/%RH	Not Measured	Not Measured	Not Reported	[43]
PEDOT:PSS + Fe_2O_3	Polymer-Metal Oxide	4 Electrodes on Substrate	Relative Resistive	30-70 %RH	0.63%(ΔR/R)/%RH	>1 second	>1 second	Not Reported	[44]
PEDOT:PSS (5%)+	Polymer-Metal Oxide	IDT with SAW effect	**Impedance + Capacitive**	0-80 %RH	81 Ω/%RH .33 pF/%RH	**~0.2 seconds**	**~0.52 seconds**	**± 1.02%**	**Current Work**

$ZnSnO_3$(5%)									
PEDOT:PSS (10%)+ $ZnSnO_3$(5%)	Polymer-Metal Oxide	IDT with SAW effect	**Impedance + Capacitive**	0-80 %RH	188 Ω/%RH .30 pF/%RH	~0.625 seconds	~0.53 seconds	± 2.20%	Current Work
PEDOT:PSS (5%)+ $ZnSnO_3$(10%)	Polymer-Metal Oxide	IDT with SAW effect	**Impedance + Capacitive**	0-80 %RH	350 Ω/%RH .28 pF/%RH	~0.63 seconds	~0.56 seconds	± 2.35%	Current Work
Note: The cells with "bold and highlighted" categories indicate the best performance in the particular category.									

2.2. Fabrication of $ZnSnO_3$ based Humidity Sensor onto Arbitrary Substrates by Micro-Nano Scale Transfer Printing

A flexible humidity sensor has been fabricated by a transfer printing technique. The device is fabricated by spin coating a composite of an equal (1:1) wt% ink of poly(3,4-ethylenedioxythiophene) polystyrene sulfonate (PEDOT:PSS) and zinc-stannate ($ZnSnO_3$) on a water soluble substrate (WSS), screen printing silver interdigitated (IDT) electrodes and spin coating low modulus Polydimethylsiloxane (PDMS) on top of the IDTs. The water soluble substrate is then dissolved and removed and the device is laminated onto an arbitrary substrate in an inverted configuration. The device performance has been tested by transferring onto curved plastic substrates with different radii of curvature R_c. The devices show impedance change from ~18MΩ to ~1.8MΩ from 0% to 90% relative humidity (RH) with a negligible variation in results, over different bending radii. The transfer printing technique reported here would provide efficient and reliable route for the fabrication of flexible electronics on nonconventional substrates in environmental sensing, soft robotics, and artificial skin etc.

2.2.1. Introduction

An increasing number of electronic devices require practical and effective methods for transferring microelectrodes and nanomaterial based thin films onto arbitrary substrates. These transferred devices in turn show significant features like bendability, conformability, and robustness, which are imperative for wearable, implantable, and biological environmental sensing devices.

The most important step in the fabrication of IDT based devices is the fabrication of electrodes, which is done using various printing techniques, such as screen printing, roll-to-plate offset printing, electrohydrodynamic (EHD) printing, and inkjet printing. The next step is the deposition of the active thin film on top of the IDTs, which is usually done by spin coating[25], dip coating, electrohydrodynamic atomization (EHDA), slot-die coating, roll-to-roll micro-gravure coating, etc. All of these printing and deposition techniques require a flat substrate and lack the ability to print material directly onto arbitrary substrates such as plant leaves, egg shells, human skin, textile fabrics, and various other curved surfaces. Therefore, there is a great need for a transfer mechanism which can enable the devices fabrication on non-flat arbitrary substrates.

So far, transferring thin film structures and devices onto arbitrary surfaces/substrates has been quite challenging. Transferring techniques such as peel-and-stick[45,46], PDMS stamping[47–50], peeling and casting[51], water assisted transfer printing[52], thermal release tape (TRT) transferring[53], in-situ transferring in water[54], push coating[55], nitrogen gas pressing[56], gecko-printing[57], mechanical force[58], Au-carrier transfer printing film[59], and a few others have been used by many researchers. The above mentioned techniques are used for transferring thin films[46,60], micro-patterns[61], nano-wires[62] and multilayered devices[63] onto arbitrary substrates.

Several humidity sensors have been reported by researchers based on Quantum Dots [64], CNTs[65], Nanorods [66], thin films [67], nanoparticles [39], conductive polymers [1], and nanocomposites [68]. PEDOT:PSS is a conjugate polymer and is widely used in transparent conductive electrodes and also for humidity sensing[16]. PEDOT:PSS hybrid thin films have been transferred using in-situ water transfer printing method[54] , onto PDMS by creating trench type roughness[69] and random micro ridges[70]. Ag films have also been deposited on PDMS by creating random micro ridges[71]. A detailed comparison of transfer mechanisms for transferring a wide range of electronic patterns, thin films, and complete devices has been provided in the table 2.2.

In this work, we have fabricated a humidity sensor from a nano-composite of PEDOT:PSS and $ZnSnO_3$, and transferred it onto various arbitrary shapes using water-assisted transferring technique. In order to compare the performance of our sensors on different bending radii, the humidity sensing response was analyzed after transferring to curved plastic substrates with different radii of curvature. The transfer mechanism efficiency has been evidently reported by the commendable performance of humidity sensors independent of the radius of curvature of the target substrate.

2.2.2. Experimental

Synthesis of Materials

The cubic crystals of zinc stannate ($ZnSnO_3$) used for this study have been synthesized by a hydrothermal process[26] from zinc sulphate heptahydrate ($ZnSO_4 \cdot 7H_2O$) and sodium stannate trihydrate ($Na_2SnO_3 \cdot 3H_2O$) precursors. The precursors were purchased from Duksan pure Chemicals, and SAMCHUN pure Chemicals Co., Ltd, South Korea. The formation of $ZnSnO_3$

nanocubes has been confirmed by the XRD spectrum (Figure S1), and SEM image (Figure S2). The XRD spectrum indicates the formation of pure $ZnSnO_3$ nanocubes without any impure phases. FE-SEM image of the as prepared $ZnSnO_3$ nanocubes show their cubic structure and uniform size. PEDOT:PSS in the form of solvent based paste with 3 wt% solid contents was obtained from Orgacon.

The nano-composite ink of PEDOT:PSS and $ZnSnO_3$ was prepared by mixing the two materials in IPA(Isopropyl alcohol, C_3H_8 , purity ≥ 99.5%) in an optimized ratio i.e 1:1 wt% (details are mentioned in our recently published work[72]). Water soluble polyvinyl alcohol (PVA) film (30µm thickness) was purchased from KURARY POVAL FILM Co, Ltd, Japan. PDMS used was sylgard® 184 silicone elastomer kit, purchased from DOW CORNING. The base polymer (part A) is mixed with the curing agent (part B) in a 30:1 ratio in a beaker and mixed vigorously by a plastic rod for 2 min. The mixture was subjected to subsequent degassing in a degasser until all the bubbles were removed. The Ag nanoparticles conductive ink for screen printing was purchased from PARU with particles diameter range of 20~200 nm, Ag contents of 80~88 wt% and typical resistance of 2.0 mΩ/sq/mil.

Sensor Fabrication

The device fabrication started with laminating a 30 µm PVA water soluble substrate (WSS) on a glass substrate in order to support the surface of flexible PVA film. The glass substrate was cleaned by chemical etching using Acetone followed by UV cleaning prior to laminating PVA on top of it. The device architecture is shown in Figure 1(f and i) in its inverted and upright positions to demonstrate that the device will be in upright position after dissolving the PVA film. The sensing layer (PEDOT:PSS + $ZnSnO_3$) was spin coated using ACE-200 spin coater on WSS at 1300 revolutions per min for 30 s. The sample was then dried in an oven (SciLab™ SOF Ovens Forced

Convection-type) at 120 °C for 3 h. The subsequent layer of 5 pairs of Ag IDTs was fabricated by screen printing using a semi-auto screen printer (SUNMECHANIX, Korea). The distance between two consecutive electrode fingers and the width of each electrode is 450 μm each as shown in Figure 2(b). The Ag IDTs were then cured in the oven at 100 °C for 30 min. The printed IDTs on top of the sensing layer on WSS are shown in Figure 2.

Transfer Printing Mechanism

The schematic illustration of step-by-step transfer mechanism of the device is shown in Figure 2-2-1. After the printing of Ag IDTs on the sensing layer, the receiving substrate of PDMS elastomer was deposited by spin coating the gel blend at 3000 rpm for 30s. The PDMS films were then cured at 100°C for 3 h in an oven. The auxiliary view (Figure 2-2-1e) and side view (Figure 2-2-1f) show the layered structure of the device. The top surface of the ultra-low modulus PDMS is highly sticky, so it can be attached to any arbitrary substrate with high conformability. The device is then delaminated from the glass surface (Figure 2-2-1 g and h), and flipped upside down to get the upright configuration of the device with the water soluble PVA layer on the top surface. The PVA layer is eventually removed by dissolving in DI water at 60 °C for 20 minutes (Figure 2-2-1, j). The final device with PDMS as substrate is then dried in oven at 60°C for 20 minutes to completely remove the water from the device. At this stage the device is ready for transfer to any arbitrary substrate.

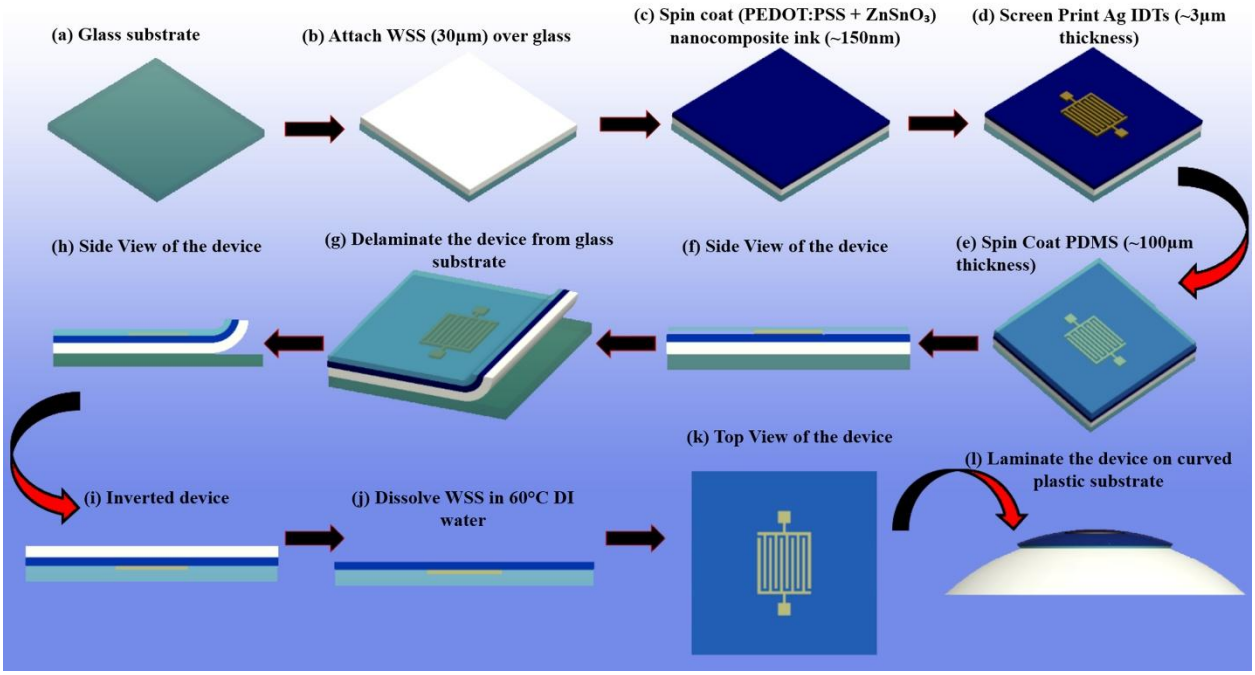

Figure 2-2-1**:** Device architecture and Schematic illustration of transfer mechanism steps.

In Figure 2-2-2 (a,b, and c) Ag nanoparticles IDTs printed on PET substrate are shown along with the comparison to the same ink printed on water soluble substrate. It can be clearly seen from the figure, that there are negligible defects in the IDTs printed on water soluble substrate.

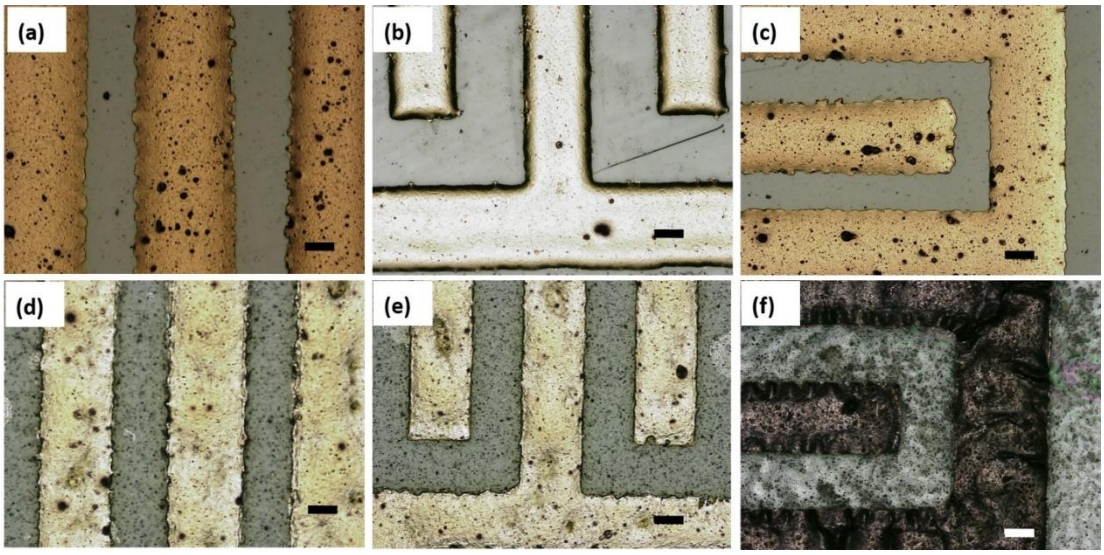

Figure 2-2-2**:** Microscopic images of Ag IDTs at 5X magnification on PET (a,b,c) and on water soluble substrate (d,e,f). Scale bar = 200µm.

The post-transfer microscopic analysis of device has been shown in figure 2-2-3. The nanocomposite material is on the top of Ag IDTs as per our device structure. There are no visible defects in either the active sensing layers or the IDTs.

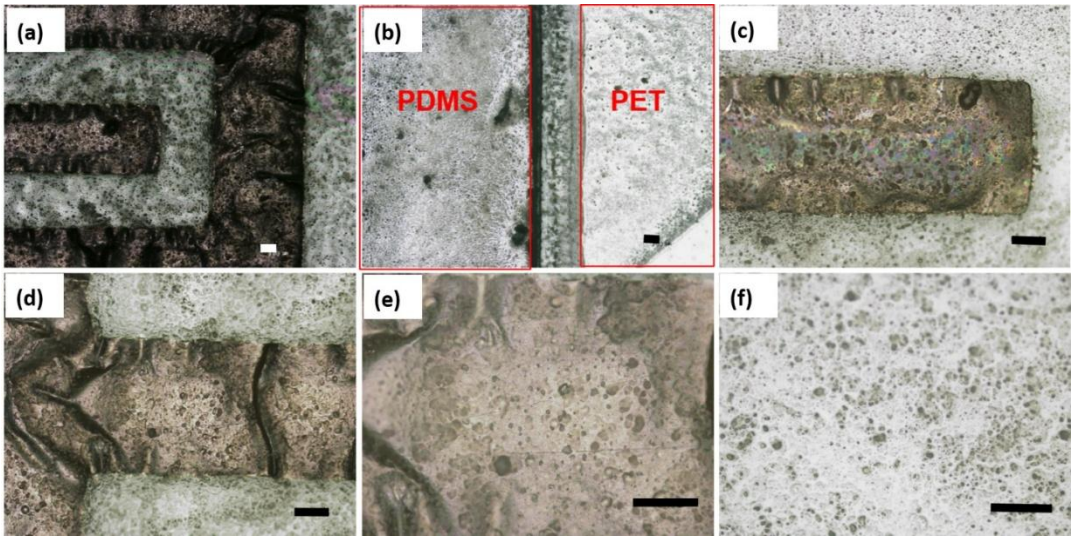

Figure 2-2-3**:** Microscopic Images of humidity sensor device on PDMS (a) IDTs and (PEDOT:PSS+$ZnSnO_3$) @ 5X (b) (PEDOT:PSS+$ZnSnO_3$) @ 5X (c) IDTs and (PEDOT:PSS+$ZnSnO_3$) @ 10X (d) IDTs and (PEDOT:PSS+$ZnSnO_3$) @ 10X (e) IDTs and (PEDOT:PSS+$ZnSnO_3$) @ 20X (f) (PEDOT:PSS+$ZnSnO_3$) @ 20X.

2.2.3. Characterization of Sensing Layer and IDTs

The surface morphology was analyzed through a NanoView high accuracy non-contact surface profiler (Figure 2-2-4 (a-c)). The 2D surface profiles for PEDOT:PSS and $ZnSnO_3$ composite thin films on WSS and on top of IDTs transferred on PDMS have been shown in figure 2-2-4 panels a and c respectively. It is obvious in the 2D and 3D profiles of the composite film from Figure 4, that it is a porous film, as compared to the neat PEDOT:PSS film[72]. This porosity is favorable for the humidity sensing, as it plays a great role in making the film hydrophilic and increasing the active sensing surface are of the film.

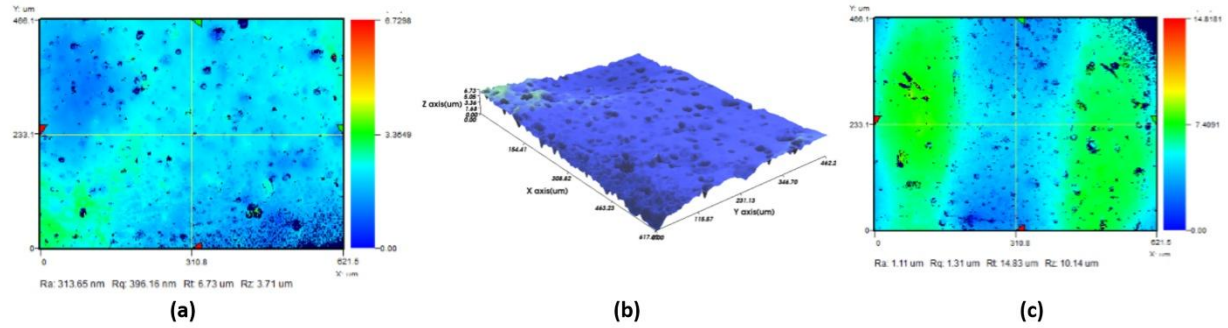

Figure 2-2-4. 2D and 3D surface profiles. (a) 2D surface profile of composite material on WSS, (b) 3D profile of composite material on WSS, (c) 2D surface profile of complete device on PDMS substrate.

The thickness of the fabricated nano-composite film was ~150nm as measured by state-of-the-art, nondestructive, Ellipsometry system (K-MAC Spectra Thick Model: ST4000-DLXn)and was confirmed by the cross-sectional SEM image presented in Figure 2-2-5.

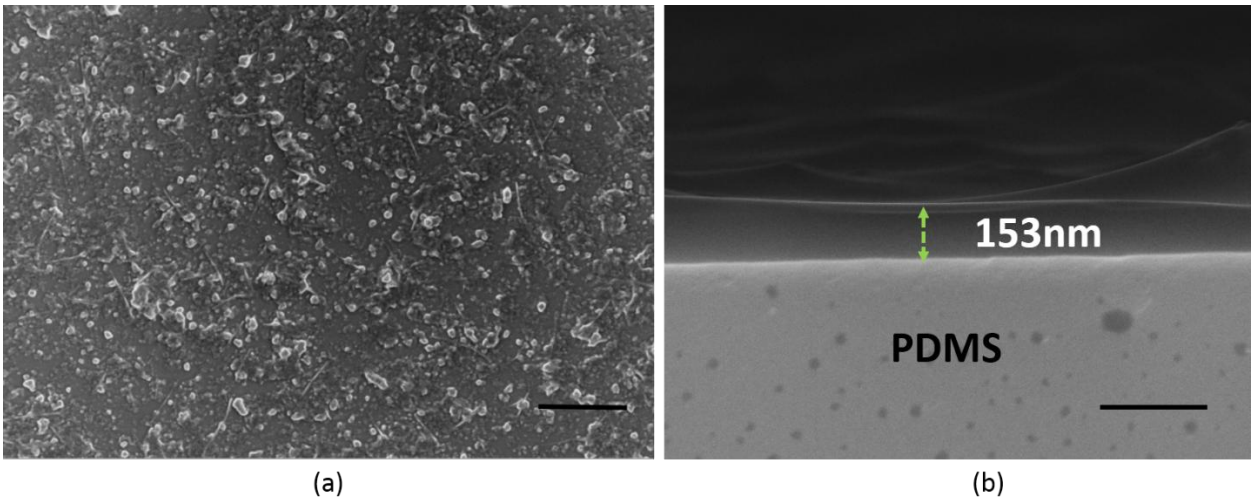

Figure 2-2-5: SEM images of the fabricated films. Surface SEM profile of the nano-composite film, scale bar = 500nm (a), Cross-sectional SEM image of the film on the PDMS surface(b), scale bar = 300nm.

The chemical structure of PEDOT:PSS and $ZnSnO_3$ is shown in the Figure 2-2-6 a and b. The Fourier transform infrared radiation (FTIR) spectroscopy of the Nanocomposite material was studied for the chemical and elemental footmarks of $ZnSnO_3$ and PEDOT:PSS in the nano-composite film.In Figure 2-2-6(c), the peaks observed at 540 cm^{-1}, 587 cm^{-1}, and 1110 cm^{-1} show the presence of M-O or M-O-M groups which are characteristics of $ZnSnO_3$[30]. The bands at 830 cm^{-1} and 949 cm^{-1} show the presence of S-C bonds in PEDOT chain[31]. .

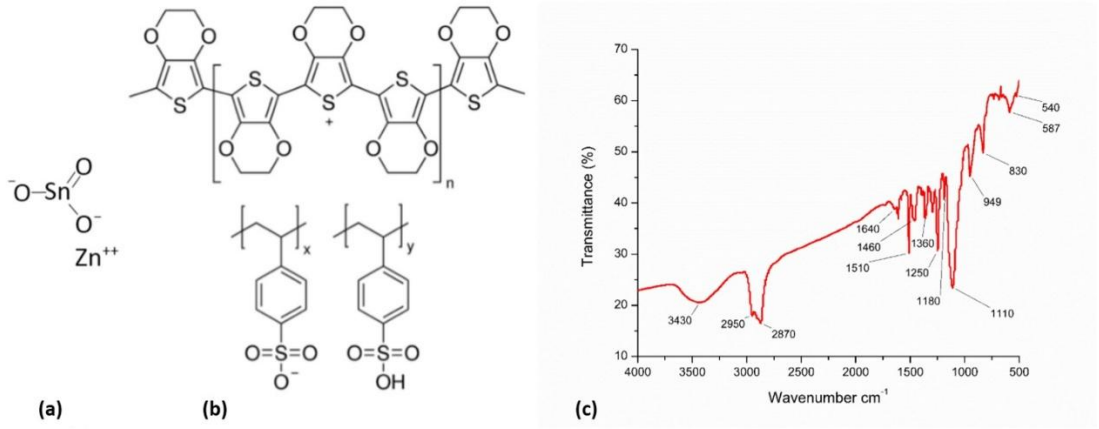

Figure 2-2-6: Chemical formulae of sensing layer materials. (a) $ZnSnO_3$ (b) PEDOT:PSS and (c) Fourier transform infrared radiation (FTIR) spectrum for the sensing layer composite materials ($ZnSnO_3$ and PEDOT: PSS)[72].

2.2.4. Humidity Sensing Response

Humidity sensing response of the sensor was studied in an in-house developed humidity chamber (Figure 2-2-7). The sensor to be analyzed was placed alongside the reference sensor inside the humidity chamber. HTU21D temperature and humidity sensor has been used as reference sensor in this setup (accuracy ~ ±2% RH, resolution ~0.04% RH, response time t_s <5 s and temperature coefficient ~ -0.15%RH/°C). The sample sensor was connected to the digital LCR meter (Applent AT825) for feedback of impedance and time to the computer via a USB data logger. The reference sensor was also connected through an Arduino based interface circuit to the computer giving the real time values of relative humidity and time inside the humidity chamber.

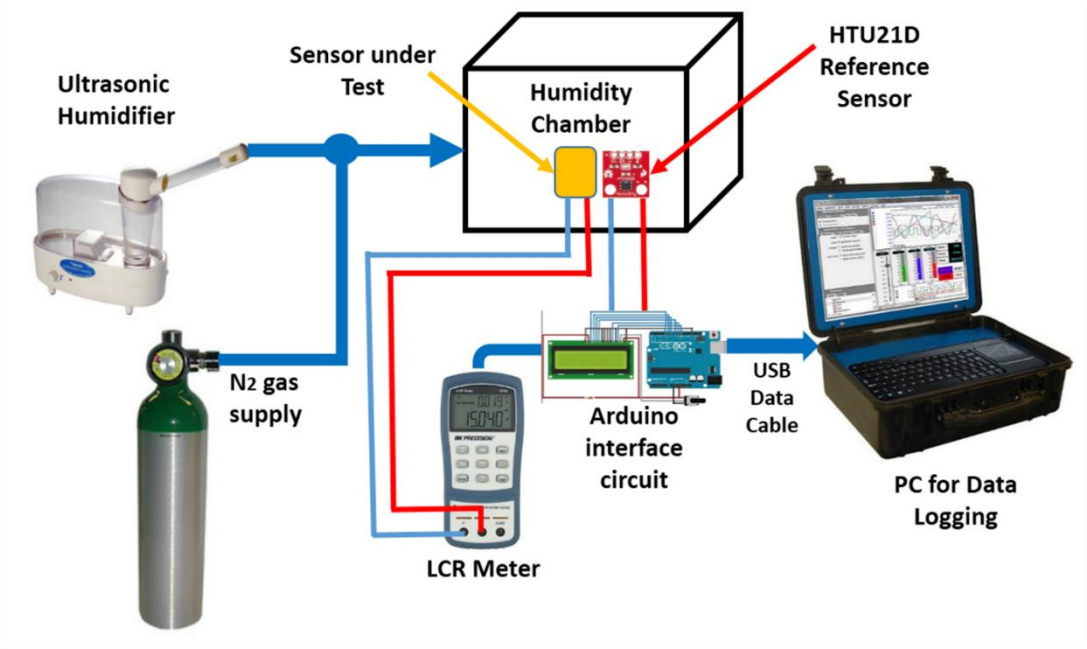

Figure 2-2-7: A schematic diagram of the humidity measurement setup showing the individual components and the humid air flow direction.

After setting up all the connections, humidity was increased using an ultrasonic humidifier and vapors were fed into the measurement chamber through feedback controlled system with reference to the commercial chamber and the data was logged one reading per second for increasing humidity level until the relative humidity reached 90%. Afterwards, the vapor supply was cut off and pure dry nitrogen gas was introduced gradually into the humidity chamber to slowly decrease humidity back to 0%. The same procedure was repeated to get the response of the sensor for the whole range of adsorption and desorption of the humidity and to see the hysteresis effect in the sensor response. One complete cycle of adsorption and desorption took approximately 20 min.

2.2.5. Results and Discussion

The fabricated sensors were transferred onto various arbitrary substrates as presented in Figure 2-2-8. After the water soluble PVA sacrificial layer was removed by dissolving in DI water, the electronic devices on PDMS membranes were transferred manually onto the target substrates with arbitrary shapes and surface structures. The adhesion of ultra-low modulus PDMS is strong enough

to stick and hold onto any kind of surface ranging from polished smooth surfaces to highly rough substrates. In Figure 2-2-8 we have shown the transferred electronics onto non-conventional substrates like plant leaf, sea crab with random up and down surface, gloved finger, ballpoint pen, wings of a dragon fly, and three rough surfaced flat and semi-spherical plastic substrates fabricated through a 3D printer. The three plastic substrates i.e., the flat substrate (Figure 2-2-8f), and two curved substrates with radii of curvature 80mm (Figure 2-2-8g), and 60mm (Figure 2-2-8h), were used to test the device performance at different bending angles.

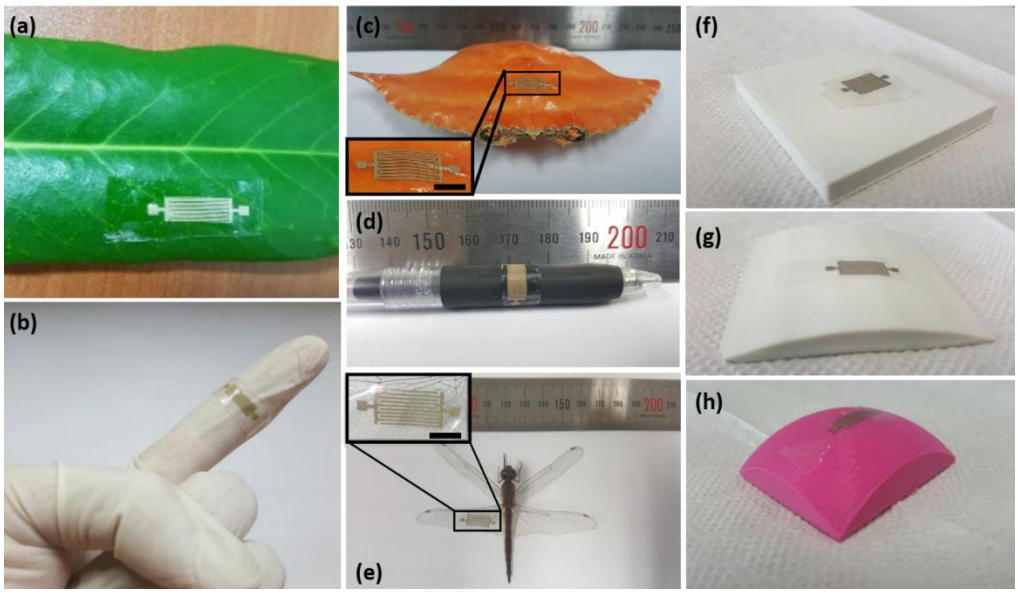

Figure 2-2-8**:** Real images of transferred devices on arbitrary curved and slanted surfaces, (a) Plant leaf, (b) gloved finger, (c) shell of a sea crab: scale bar = 5mm (d) cylindrical surface of a ballpoint pen, (e) wing of a dragon fly: scale bar = 5mm, and rough plastic substrates having radii of curvature (e) $R_c = \infty$, (f) R_c = 80mm (g) R_c = 60mm.

The performance of the sensors was investigated by measuring the impedance response of the sensors towards varying humidity levels ranging from 0% to 90% RH. The test frequency used for the response measurement was fixed at 10 kHz for all the readings. The response curves are presented in Figure 2-2-9.

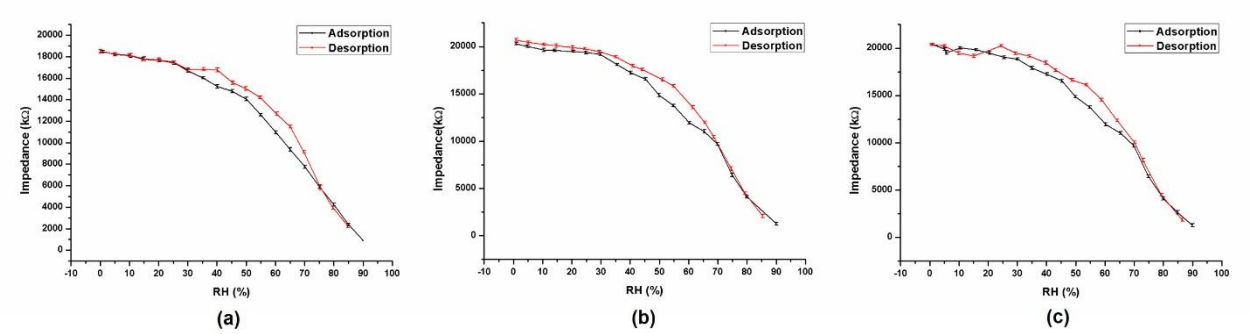

Figure 2-2-9: Impedance vs RH adsorption and desorption curves of humidity sensors on rough plastic substrates. (a) Flat substrate (b) curved substrate with R_c = 80mm, (c) Curved substrate with R_c = 60mm.

As seen from Figure 9(a), the impedance response of the sensor after transferring it to the test substrate 1 (flat plastic) for the specified full range of humidity variation is quite stable and well predicted for a $ZnSnO_3$ based humidity sensor[72]. The impedance of the sensor changes from 18MΩ to 1.8 MΩ for the full range for increasing humidity. The same sensor was then transferred to test substrates 2 (R_c = 80mm) and 3 (R_c = 60mm) that are semi-spherical substrates and the impedance response of the sensors was recorded for the full range of humidity to evaluate the device performance after transferring to curved surfaces that is the real challenge in transfer printing. Figure 9(b) shows the impedance response of the sensor after transferring it to the test substrate 2. As expected, the overall curve shape remains similar to the initial response of the sensor before transferring but the overall impedance of the sensor increased by approximately 1.15 times due to micro level deformations in the device layers during transferring process[73]. The change in impedance is quite negligible and depicts the successful transferring of the device onto a curved substrate without damaging the device or effecting the performance. Figure 2-2-9(c) show the device performance after being transferred to curved test substrate 3. As it is clearly visible from the graphs that there is no major effect on the device performance and the intrinsic device impedance, nor the Z-RH curve shape and behavior, even after being bent and transferred to curved substrates 2 and 3. The overall intrinsic impedance increased by a negligible factor as expected

because of the formation of micro deformations in the film through bending. Apart from that, the overall device response remains excellent in all conditions and on all types of target test substrates.

Based on the characterizations, results, and discussions, a hierarchical table has been formulated presenting the comparison of the printing/fabrication methods, device substrate, transfer mechanism, and percentage yield of the devices presented in this work and the previously carried out research works using different type of transfer mechanisms and fabrication techniques. The detailed comparison presented in supplementary Table 2.2 shows that most of the devices are fabricated by conventional fabrication techniques like photolithography, e-beam evaporation, CVD, and shadow masking.

Table 2.2 Summary of the transfer printing mechanisms of a wide range of electronic devices

Devices/ Applications	**Transfer Mechanism**	**Transfer type**	**Device Substrate**	**Device Fabrication Method**	**Percentage Transfer Yield**	**Reference**
IDT based humidity sensor	Dissolving sacrificial water soluble substrate	Water soluble sacrificial layer	PDMS	Screen printing, spin coating.	~100%	This work
Solar cells, Photodiode	Stamping and Peeling	PDMS Stamping	MgO, mica, graphite	Photolithography, electron beam evaporation	-	[49]
OTFT	Dry printing (Adhesion and Cohesion)	Differential adhesion	PET	Photolithography, Spin coating	-	[74]
Solar Microcells	Casting and Peeling	PDMS Stamping	PDMS	Optical Photolithography, Spin coating	~99.9%	[48]
Transparent TFTs	Transferring and peeling	Thermal release tape	ITO Coated PET	Photolithography, CVD, Liftoff.	~100%	[75]
TFTs	Plasma-Assisted stamping using Si stamp	Stamping	PET	Spin coating, vapor deposition, lithography.	~95%	[76]
Transistors	Deterministic assembly	PDMS stamping	Silicon wafer	Photolithography, PECVD.	~100%	[77]
Stress Sensors, Pressure sensors	Transferring and peeling	Thermal release tape	PDMS	Photolithography	50-70%	[78]

OFET based Flexible Pressure sensors	Casting and Peeling	PDMS casting	ITO Coated PET	Shadow masking, thermal evaporation.	-	[51]
NW Devices (Resistors, Diodes, FETs)	Thermal release tape, peel off in water.	Water-assisted transfer printing method	PI, PDMS, glass, paper.	Photolithography	~100%	[52]
CNT based TFTs	Gold carrier film as sacrificial layer	Chemical Etching	PET	Photolithography, CVD.	~100%	[59]
Phase-change chalcogenide material structure	Laser Induced Forward Transfer	Laser-direct-writing process	Glass	Magnetron sputtering, femtosecond lase lithography	~100%	[79]
Polymer TFTs	PDMS-based stamp pressing and peeling	Push coating	SiO_2	Photolithography	-	[55]
TFSCs	Water assisted Peel-and-stick process	Thermal release tape	Cell phone, paper, plastics, textile.	e-beam evaporation, Plasma enhanced CVD	~95%	[46]
Flexible/ Transparent thin-film electronics	Water assisted Peel-and-stick process	Water-assisted transfer printing method	Polyimide, flexible plastic.	PECVD, e-beam evaporation, spin coating.	~100%	[45]
Transistor TFTs	Dissolving water soluble layer and stick the device to desired substrate.	Water-assisted transfer printing method	Polyimide foil, polypropylene foil, Skin, Plant leave, textile.	Thermal evaporation, spin coating	85%	[80]
Graphene films	Lamination and copper etching	Direct transfer method	Paper, PVC, PET, Cloth, Polycarbonate	CVD, Lamination using heated rollers	-	[81]
EP sensor, Temp sensor, Strain sensor	PVA dissolving, and elastomeric stamp	Water-assisted TP, and Stamping.	Human skin, PDMS replica of skin, Polyimide.	Photolithography, dry etching, e-beam evaporation	~100%	[82]
Cutaneous pressure monitoring sensor	Stamping and retrieving	PDMS stamping	Ecoflex	Reactive ion etching, PECVD.	~80%	[47]
Graphene Transistors	Nitrogen gas pressing through sample holder	Pressing and peeling	Polyimide	CVD, spin coating, e-beam evaporator, shadow masking.	-	[56]

CNTs and Graphene hybrid thin films	PAA dissolving as a sacrificial layer	Water-assisted transfer printing method	PET	Vacuum filtration	-	[54]
Lactate sensor	Direct assembly by offset transfer printing	Offset printing	PEN	Photolithography, Liftoff, Electrophoresis	-	[83]
Wearable RGB QDLED, PWQLED arrays.	PDMS stamping using intaglio trench	Intaglio transfer printing	PET	Thermal evaporation, spin coating	~100%	[84]
Stretchable TFTs (Ag NWs, CNTs, elastomeric dielectric	Overcoat, cure elastomer, peel off device and laminate.	Casting and peeling elastomer, Lamination	PUA polymer	Spray painting, shadow masking	85.7%	[85]
GMR sensor	Dissolving water soluble PAA layer	PDMS casting and peeling	PDMS	Lift-off photolithography	-	[86]

Based on the type of device, type of transfer mechanism, substrate used, process of fabrication, and percentage yield, a hierarchical table has been formulated presenting the comparison of different transfer printing methods. This transfer printing technique ensures the complete transfer of layered devices onto a wide variety of substrates with full functionality, and ease in fabrication.

2.3 Reverse Offset printed environmental friendly sucrose based temperature sensor

An all printed interdigitated electrodes (IDT) based temperature sensor has been demonstrated in this study. The IDTs were fabricated on a glass substrate by reverse offset printing. The sucrose film was fabricated by spin coating the sucrose solution on the IDTs. The sensors showed stable and close to linear response of resistance change by varying temperature in the range 0°C to 100°C. The resistance of the sensors changed from ~3200kΩ to ~400kΩ for the temperature change in the range 0°C to 100°C. This study provides an effective method to fabricate temperature sensors with higher performance based on thermistor effect in the future.

2.3.1. Introduction

A measure and control of temperature in an ambient atmosphere is important for our daily life, industrial processes, and environmental monitoring. The thermistor based temperature sensor is one of the most important candidates for temperature sensing that has outstanding advantages of immunity to electromagnetic interference, simple fabrication, cost-effectiveness, and durability against harsh environments. Thermo resistive devices are extremely sensitive to the external temperature; therefore, by applying thermo resistive based material a temperature sensor with high sensitivity and practicability can be obtained.

Organic and disposable sensors have great potential for applications such as food industry, environmental monitoring and medical industry. Various types of temperature sensors have been fabricated , which include thermocouples[87], nanogenerators based temperature sensors[88], and thermistors[89,90]etc.

Thermoplastic polymer composite containing metallic filler based thermistors have been used as temperature sensors[91], which show linear response from 20°C~200°C. Polydiacetylene thermoresponsive fluorogenic supramolecules have been used as temperature sensor in microfluidic devices[92]. An extremely simple thermocouple made of a single layer of metal has been fabricated by photolithography[87]. Lead zirconate titanate (PZT) single micro/nanowire pyroelectric nanogenerator has been utilized as self-powered temperature sensor[88]. PE/PEO binary polymer composite with Ni microparticles has been reported to be used as flexible wireless temperature sensor[93]. Pentacene/Ag NPs based high resolution OTFT has been used as a high dynamic range thermistor[94]. PEDOT:PSS-CNT film on PET substrate has been used as a temperature sensor in artificial electronic whisker[95].

The evolution of modern science and technology has created new demands for accurate measurement of local temperatures in various conditions. This has sparked the development of novel thermal sensors at scales down to micro- and nano- meter, and in a variety of environments, from outer space to the interior of living cells [1-9]. However, no matter whether conventional resistive temperature detectors (RTDs) or the latest light-induced-luminescence thermometers are used [7], active sensing modes or complicated structure/interface configurations in these devices limit their application, for instance in built-in sensors for small-scale devices, in flexible substrates, or in harsh environments.

At present, the traditional thin- film based processing is quite mature, which has been used successfully in semiconductor technology over the past few decades and led to advancement of modern portable electronics and optoelectronics. Considering the technological compatibility, piezoelectric semiconductor thin films can be a good candidate to substitute 1D nanostructures for realizing piezotronic applications. There are various methods for growing piezoelectric semiconductor thin films, such as physical vapor deposition [15,16], wet chemical deposition [17,18], radio frequency (RF) sputtering[19], molecular beam epitaxy[20], and metal−organic chemical vapor deposition.

In this paper, we present the study of thermoresistive effect in sucrose coated on IDTs on a glass substrate. The sucrose film is integrated on highly sensitive IDTs whose resistance changes dramatically once the temperature changes.

2.3.2. Experimental

The sucrose solution was synthesized by simply dissolving table sugar in DI water. 5wt% of sucrose was dissolved in 10ml of DI water in a glass bottle using a magnetic stirrer for 1 hour at 50°C and 1000 rpm.

The device fabrication started with printing of Ag IDTs on glass substrate using Reverse offset printing. The Printed IDTs with 20 pair of IDTs, and 50µm width and gap in each electrode is shown in figure 2-3-1.

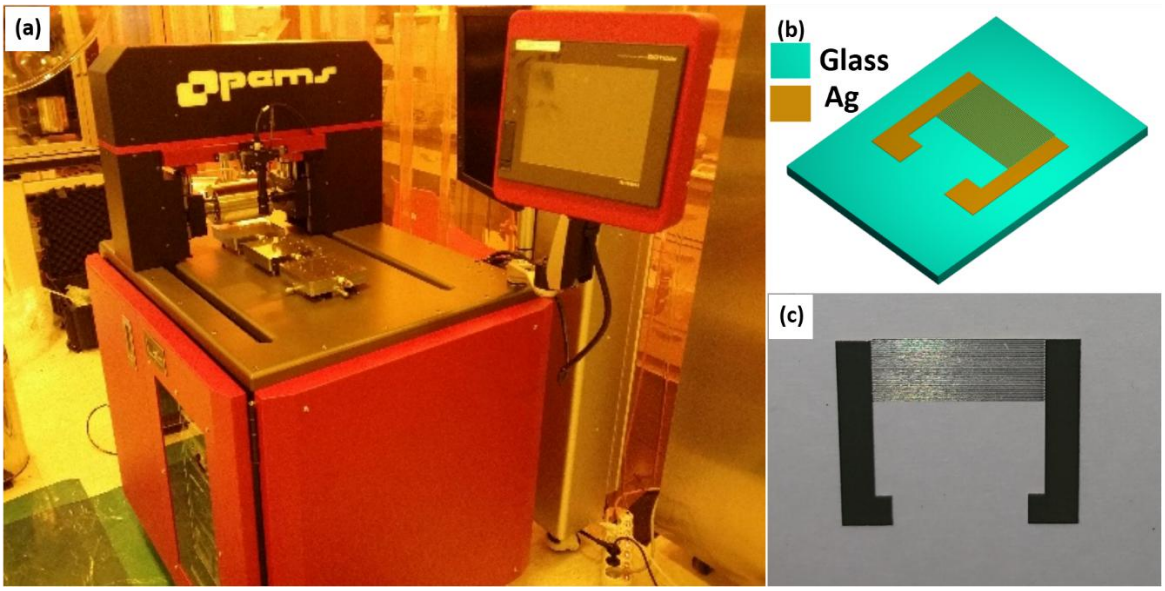

Figure 2-3-1: (a) Real photograph of reverse offset printing system, (b) CAD design, and (c) real photograph of the Ag IDTs printed on glass.

The whole process of reverse offset printing system includes a glass slide to deposit ink, a roller enfolded with a blanket of highly hydrophobic poly-dimethylsiloxane (PDMS) material, a cliché containing the negative of electrode patterns acutely carved in its surface in the form of trenches and finally the chosen substrate for device fabrication. Whole printing process is presented step by step in figure 2-3-2. Initially Ag ink was spin coated on a coating substrate (glass slide in our case) at 3000 rpm as shown in figure 2-3-2(a,b). The PDMS blanket roll was rolled over the spin coated Ag ink glass slide to attach a thin yet uniform layer of Ag ink owing to the high absorption coefficient of PDMS as shown in figure 2-3-2c. Ink coated PDMS blanket roll was rolled over the cliché surface with optimized speed and pressure to transfer the electrode patterns on it by leaving all the unwanted Ag ink on the cliché surface owing to its higher value of adhesion coefficient (Off Process). The design of cliché with the negative of bottom electrodes engraved in

its surface and all unwanted ink on its surface is shown in figure 2-3-2d. The blanket roll was rolled over the desired glass substrate as the final step of printing high quality Ag electrodes (Set Process) as shown in figure 2-3-2 (e & f).

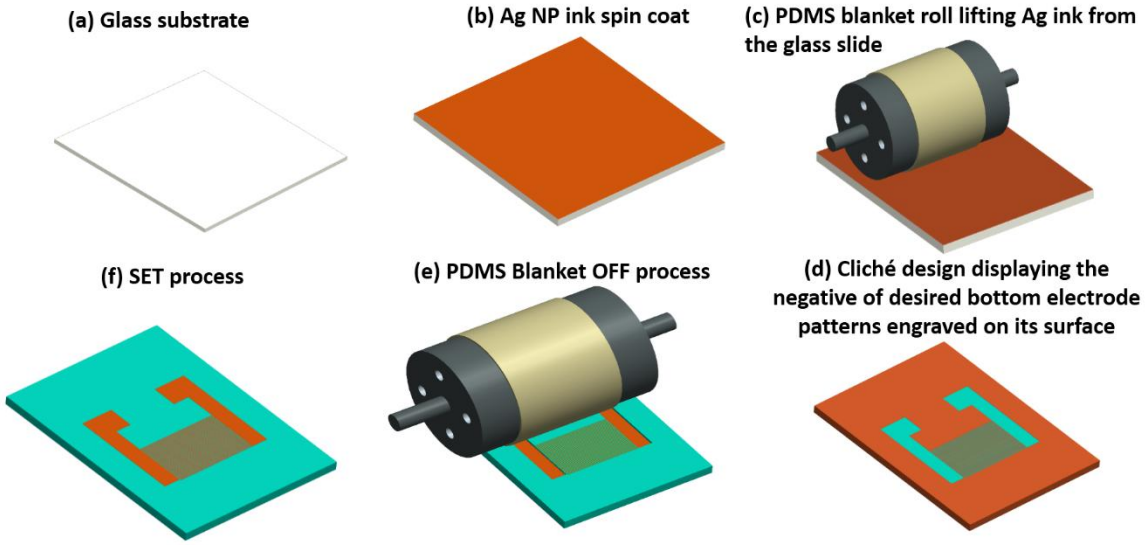

Figure 2-3-2: Schematic illustration of Reverse Offset printing of Ag IDTs on glass substrate.

Extremely fine bottom Ag electrodes with 100 um resolution and outstanding resistivity of 0.4 ohm-cm were realized after sintering for 1 hour at 110 °C in a furnace.

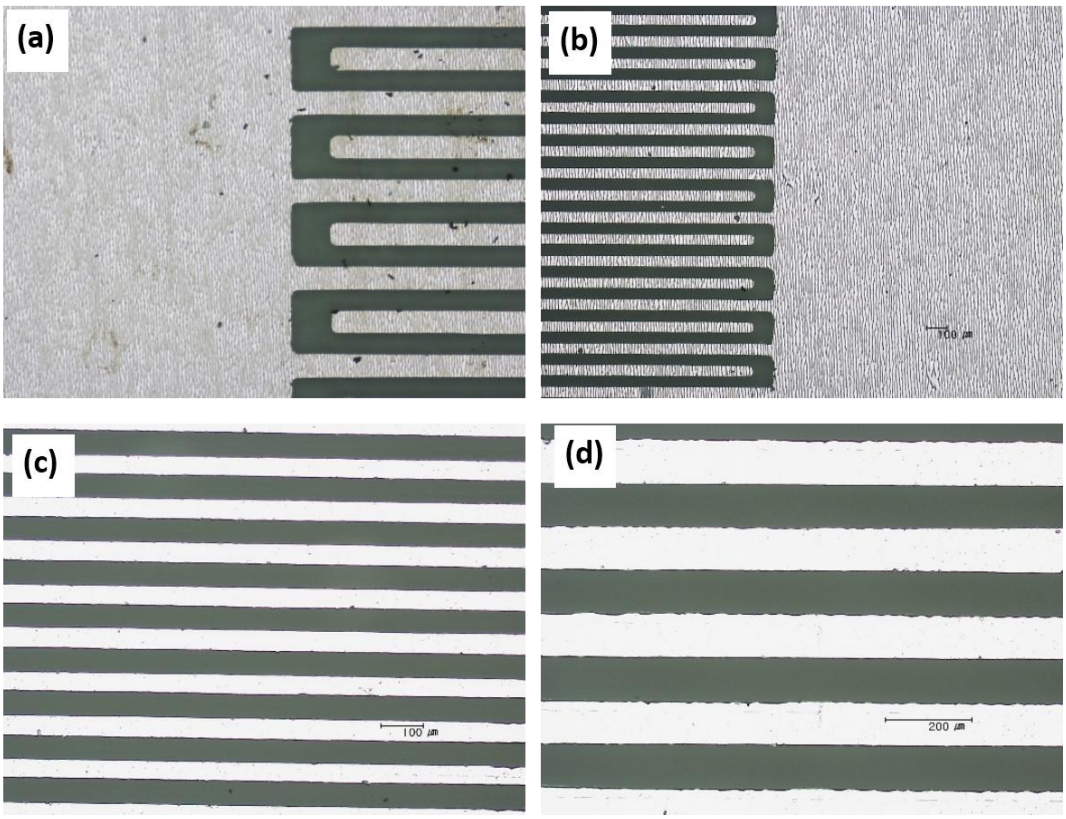

Figure 2-3-3: Microscopic images of the reverse offset printed IDTs showing the dimensions of the IDTs fingers width and gaps.

2.3.3. Electrical Characterization

The sensors were characterized for their response towards changing temperatures of a controlled environment by recording their resistance (R) variation and the trend it follows. The setup was designed and fabricated in-house to accurately and reliably record the data. The schematic diagram of the characterization setup is presented in Fig. 4. The temperature change on the surface of hot plate was controlled by using an automatic feedback controller. Temperature changes were controlled by the control panel of the hot plate. The real time readings of the temperature on the hotplate surface were displayed on an LCD and were also sent to computer through USB communication for automatic data logging.

The temperature of the hotplate was changed per step through a manual control user input and was maintained at that point until the resistance readings of the sensors were stable. The time to

stabilize resistance was given to compensate for the difference in response times of the reference sensor and the fabricated sensors and to overcome the hysteresis effect of the sensors. The sensors' response was taken for the temperature range of 0°C to 100°C where the relative humidity for the whole experiment was maintained at ~60 % RH.

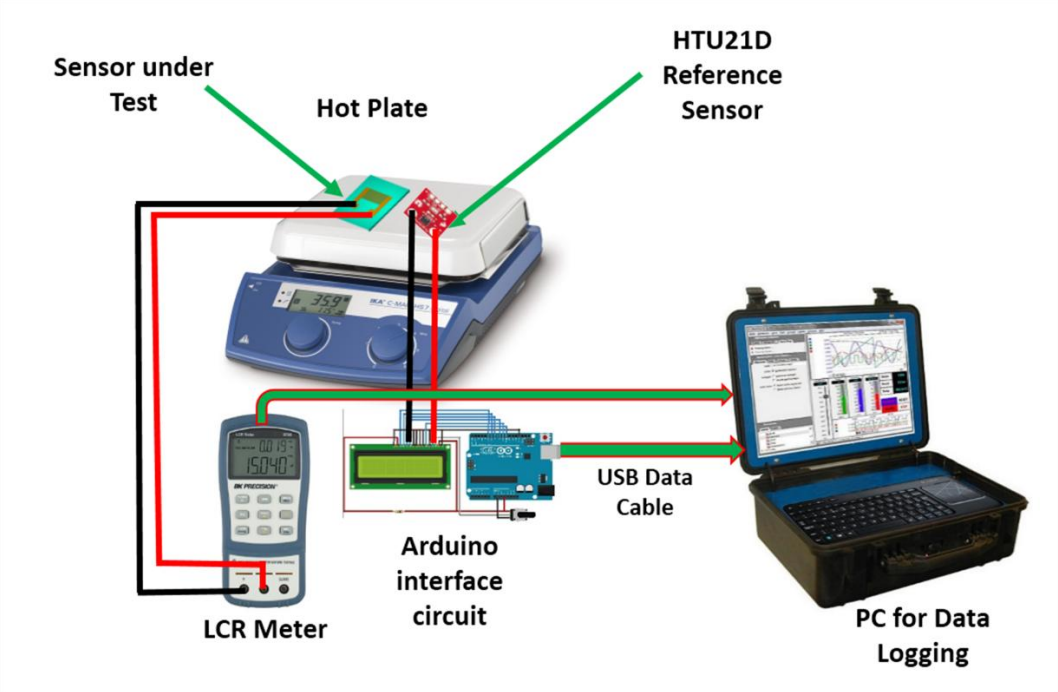

Figure 2-3-4: Schematic diagram of the in-house developed measurement setup used for recording temperature response.

After the response of the sensor was recorded, the curves were plotted in Origin Lab software.

2.3.4. Results and Discussion

The advantages of RTD sensors include small volume, high accuracy, short response time, and their capability to be mass-produced. When the temperature is increased the RTD resistance also increase and vice versa the increase of temperature results in the increase in the energies of atoms. The atoms at higher energies vibrate and there is an increase in collisions of moving electron. These collisions results in reducing the flow of electron and hence an increase in resistance is observed. This increase in resistance as shown by the following equations:

$R_t = R_i (1+\alpha_T \Delta T)$, (1)

$\Delta T = T_t - T_i$ (2)

Here ΔT is change in temperature, R_t and R_i are the resistances of the RTD at t°C and i°C and α_T is the temperature coefficient of RTD. Equation (1) can be written as

$$\propto_T = \frac{R_t - R_i}{R_i(\Delta T)} \quad (3)$$

The resistance response results presented in figure 2-3-5 indicate that the overall resistance of the sensor decrease linearly with increasing temperatures. The resistance response curves were fitted using Boltzmann second order curve fitting equations with an R^2 value greater than 0.99. This shows that the response of the sensor can easily be converted to temperature in °C with quite high accuracy by solving the equation.

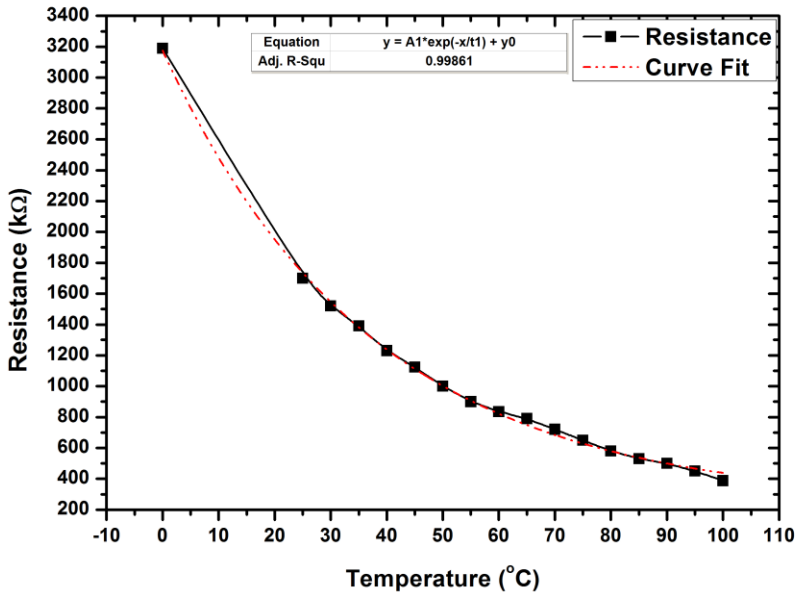

Figure 2-3-5: Temperature response in the form of resistance in kΩ as a function of temperature in °C

3. Highly sensitive flexible human motion sensor based on $ZnSnO_3$/PVDF composite

The zinc stannate $ZnSnO_3$ and Poly (vinylidene fluoride) PVDF composite has been used as a highly sensitive body motion sensor. The active layer of the composite was deposited on the PET substrate by D-bar coating. The deposited films were characterized electrically and morphologically for sensor response to bending angles and surface characteristics. The synergistic effect between piezoelectric $ZnSnO_3$ nanocubes and β-Phase PvDF endows the composite with desirable electrical conductivity, remarkable bend sensitivity, and excellent durable stability. The best recorded response of the sensor was ~20MΩ to ~100MΩ for bending angles of -150° to 0° to 150 The $ZnSnO_3$/PVDF composite show potential application in human body motion sensors under extensive bending.

3.1. Introduction

With increasing amount of research being done in the field of artificial skin in advanced robotics, strain sensing is one of the essential ingredient among other vital sensors mounted on robots.

Gestures controlled human machine interface (HMI) devices use flex sensors to operate [96–100]. Flex sensors are also implemented to interpret sign language by mounting them on gloved fingers and interfacing with signal processing circuits [101–103]. Strain and flex sensors have been applied in health monitoring to measure the muscle joint angle and muscle induced movement [104–106]. Flex sensors are simpler form of strain sensors that can only measure bending in contrast to strain sensors that are also able to measure elongation or strain in addition to bending. This simplicity makes the flex sensors easier and cheaper to fabricate as compared to strain sensors [97]. The working principle of flex sensors is based on the change in resistance of the active film upon bending angles relative to its straight position [107]**.** Another type of flex sensor is fiber optic cable based optical flex sensors. In optical flex sensors the change in bending

is observed as a change in refractive index and power output upon bending [108]**.** Two dimensional stress and flex sensors based on MOSFET have been fabricated with percentage change of only 12% and an error of 8% in output [109]**.** Flexible piezotronic strain sensor based on individual ZnO piezoelectric fine-wires have been fabricated on flexible polystyrene (PS) substrate [110]. ZnO nanorod based flexible strain sensor has been fabricated by a single-step hydrothermal reaction on Kapton substrate [111]. Flexible resistive strain sensors have been fabricated by micromolding Pd nanoparticle-Carbon on polyimide substrates [112]. SWCNTs and MWCNTs have been used for piezoresistive strain sensors due to their unique electromechanical properties [113–119]. $ZnSnO_3$ nanowire/ microwire based ultrahigh sensitive piezotronic strain sensor has been investigated by Zong Lin Wang et. al [120]. $ZnSnO_3$ NW based strain sensor showed 3 times higher gauge factor than those of CNTs and ZnO nanowires. PVDF piezo film based strain sensor has been investigated for local damage detection of steel frame buildings [121]. The use of conductive polymer composite comprising of thermoplastic polyurethane and MWCNTs as resistive strain sensors have been widely investigated by Qiang Fu et al [113]. Conductive polymer composites show a great potential in piezoresistive devices [122–125]. Highly sensitive tactile sensor based on piezoelectric conductive polymer composite of ZnO/ PVDF have been fabricated by James S. Lee et al [123]. Graphene oxide microtubes-elastomer composite based highly stretchable and ultrasensitive strain sensor has been implemented for gauging muscle-induced strain in the form of resistance change [126].

A highly stretchable strain sensor based on parallel microcracks in graphite thin film has recently shown very promising results for sensing movements of gloved fingers[127]. Inkjet printing has been used to fabricate strain sensors based on PEDOT:PSS and silver nanoparticles

on polymer substrates[128]. A stretchable strain sensor based on chewing gum and CNTs membrane has been used on gloved fingers to sense finger motions[119].

In this work, a conductive polymer composite of zinc stannate $ZnSnO_3$ and Poly(vinylidene fluoride) PVDF has been used as the active layer on PET substrate for bend sensing in both directions. Although $ZnSnO_3$ has excellent piezoelectric properties but its structure is not very robust to sustain extremely high bending angles in both directions. For this purpose, PVDF has been introduced into $ZnSnO_3$ to help in binding the $ZnSnO_3$ nanocubes together, and making the device robust, while having piezoelectric properties itself. Effect of the dimensions of sensors on the sensors' performance has been investigated. The final sensors with 3.5cm ×2cm dimensions exhibit excellent response for bend angles of -150º to 0º to 150º with ~40% reduction in normal state resistance (at 0º) for a bend of -150º, and ~60% increase for a bend of 150º. A detailed comparison of a wide range of strain and flex sensors based on material, working principle, sensitivity, stability, and durability has been provided in supplementary table 3.1 in the supplementary information.

Table 3.1: Summary of strain sensors in literature compared to our device

Device	**Material**	**Fabrication Method**	**Working principle**	**Sensitivity /Gauge factor**	**Bi-/Uni-directional**	**Maximum bending angle**	**Maximum # of cycles Tested**	**Reference**
Our device	***$ZnSnO_3$/ PVDF composite***	***D-bar coating (Rod Coating)***	***Piezoresistive***		***Bi-directional***	***±150°***	***1000***	***Current work***
Piezotronic strain sensor	ZnO NW on Polystyrene	Bonding grown wire on PS	Piezotronic Effect	G.F = 1250	Bi-directional	_	_	[110]
Flexible strain sensor	Pd NP + Carbon on Polyimide	Resistive evaporation, shadow masking	Resistive	G.F = 390	Bi-directional	_	100	[112]
Flexible strain	ZnO NR on	CVD	Resistance	_	Bi-directional	_	200	[111]

sensor	Kapton							
Piezotronic strain sensor	$ZnSnO_3$ Nanowire/ Microwire on PS	CVD for growing NW and bonding on PS	Piezotronic Effect	G.F = 3740	Uni-directional	_	_	[120]
Dynamic strain sensor	PVDF film	Prefabricated from company	piezoelectric	10mV / μstrain	Bi-directional	_	_	[121]
Stretchable strain sensor	P4VP nanofiber on PET	Electrospun with lithography	Resistivity	Sensitivity = 2.0 at Ɛ=0.03	Uni-directional	_	200	[129]
Strain sensor	PU+ MWNT on PET	Thermal setting	Resistivity	G.F = 5~140238	Uni-directional	_	_	[113]
Stretchable strain sensor	AgNW + PDMS	Drop casting, peeling	piezoresistivity	G.F = 14	Uni-directional	0° to 150°	1000	[130]
Super-Elastic strain sensor	rGO/PI	Freeze casting + Thermal annealing	Resistance	_	_	_	2000	[122]
Wearable strain sensor	CNTs + Ecoflex	Dry spun and bonded	Resistance	G.F = 0.24	Uni-directional	_	10000	[114]
Knitted Strain sensor	PU + PEDOT: PSS	Wet spinning	Resistance	G.F = -1~ -2	Uni-directional	0° to 90°	500	[131]
Multi-dimensional strain sensor	AgNW on PDMS	Photolithography	Resistance	G.F ~ 20	Uni-directional	0° to 90°	1000	[132]
Graphene strain sensor	rGO gel	Dry spinning	Resistance, current density	G.F = 20	Uni-directional	_	500	[133]
Flexible strain sensor	CNT on TPE	Filtration, peeling off	Resistive	G.F ~ 12	Uni-directional	_	100	[115]

3.2. Experimental

3.2.1. Materials

The cubic crystals of zinc stannate ($ZnSnO_3$) have been synthesized by a hydrothermal process[26] from zinc sulphate heptahydrate ($ZnSO_4 \cdot 7H_2O$) and sodium stannate trihydrate ($Na_2SnO_3 \cdot 3H_2O$) precursors. Both the precursors were purchased from Duksan pure chemicals Co., Ltd, South Korea. The formation of $ZnSnO_3$ nanocubes has been confirmed by XRD spectrum, FE-SEM

image, FTIR spectra, and Raman spectra[26]. Poly(vinylidene fluoride) (PVDF), average Mw ~534,000 by GPC, powder was purchased from Sigma-Aldrich. DMF [N,N-Dimethylformamide, $HCON(CH_3)_2$, purity ≥ 99.5%] was purchased from DAEJUNG, Korea and Acetone [CH_3COCH_3] was purchased from KANTO CHEMICAL Co., INC. Tokyo.

PVDF is a semi crystalline non-centrosymmetric polymer which exhibits piezo-, pyro- and ferroelectric properties. It is a linear polymer that shows permanent electric dipoles perpendicular to the direction of the molecular chain. These dipoles result from the difference in electronegativity between the atoms of hydrogen and fluorine with respect to carbon. Depending on the processing conditions, PVDF exhibits several different crystalline phases (α,β,γ,δ). The β phase of PVDF is the phase that exhibits the best piezoelectric properties[123].

The structure of α and β-phases of PVDF are shown in Figure 3-1 along with crystalline structure of $ZnSnO_3$.

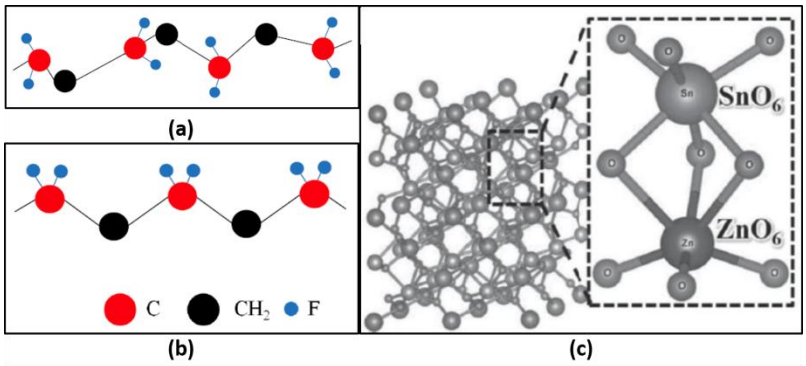

Figure 3-1: Structural formulae of α and β-phases of PVDF and crystalline structure of $ZnSnO_3$ nanocubes

3.2.2. Sensor Fabrication

Ink preparation

Ink for active layer was synthesized by making 15 wt% PVDF solution in 20ml of 1:1 DMF and Acetone as solvents. The solution was kept on magnetic stirrer at 50°C and 1200rpm for 4 hours. After the PVDF powder was completely dissolved in the solvents, 4 wt% of $ZnSnO_3$ nanocubes

was added in the solution, and the solution was stirred magnetically for overnight at room temperature. In order to get a better $ZnSnO_3$ nanocubes dispersion in the solution, the complete solution was probe sonicated for 20 minutes with 5 seconds pulse on, and 2 seconds pulse off. After that the ink was ready to be used for sensor fabrication.

D-bar coating

The sensors were fabricated solely by utilizing D-bar coating which is a simple, cost-effective, and scalable thin-film fabrication technique. The D-bar coating system is shown in Figure 3-2.

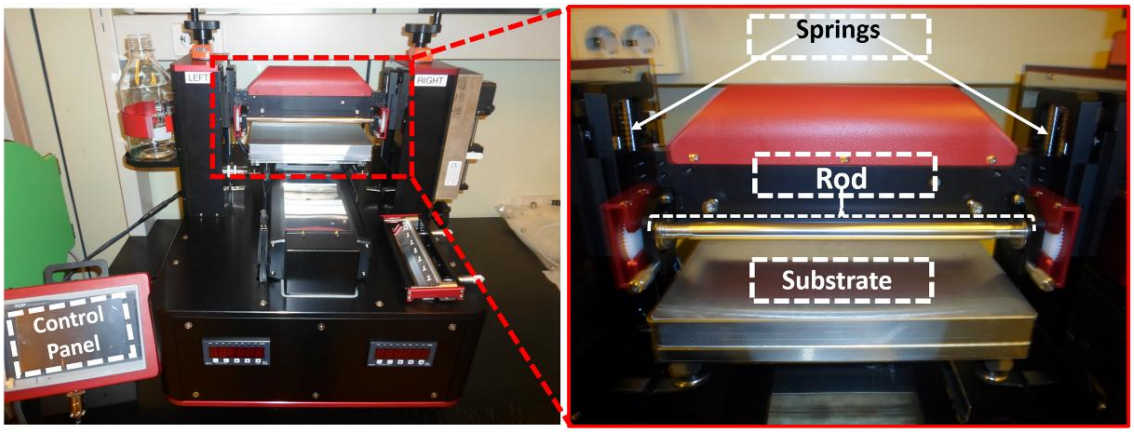

Figure 3-2: Photograph of the semi-automatic D-bar coating system. Inset showing the substrate, steel bar in the fixture, and springs for pressure control.

Figure 3-2 shows the system photograph in which a D-bar roller rolls over the substrate surface and the thickness is controlled by the gap between the steel bar and the substrate. Before depositing the sensing layer on the substrates, the strips were UV-treated for 10 minutes for better attachment of the $ZnSnO_3$/PVDF layer with the substrate. Once the substrate is placed on the platform, vacuum is turned on from the touch control panel to hold the substrate firmly and avoid slipping while the rod is rolling on the substrate. Then the rod is moved to a suitable position and height by manually adjusting the control knobs, which increase or decrease the rod height above the substrate by applying a pressure through springs as shown in inset of Figure 3-2. Ink is then poured on the steel

bar, and the bar is rolled on its axis, while not touching the substrate to fully spread the ink on its surface. Once the bar is covered with ink, it is then slowly rolled on the substrate surface. The rolling speed and linear speed of the bar is controlled from the control panel. After fabrication, all the samples were dried at 60°C overnight in an oven. After drying, the samples were then cut into strips having dimensions 3.5cm ×2cm and 3.5cm ×1cm using a sharp blade. Conductive copper tape was used to make the contacts for electrical measurements as shown in Figure 3-3 (b & c).

The schematic illustration of the fabrication process and the fabricated sensors are shown in Figure 3-3.

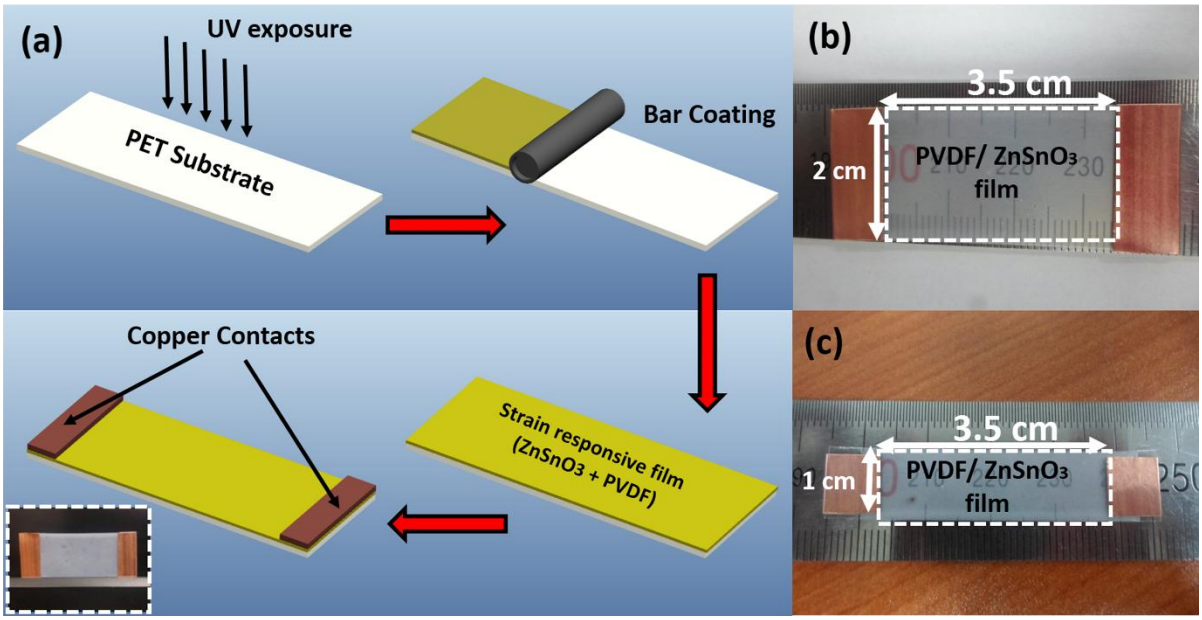

Figure 3-3: Schematic illustration of the sensor fabrication process (a), Photograph of the fabricated sensors showing PvDF/ $ZnSnO_3$ composite film with copper electrodes and two different dimensions. Inset showing the real photograph of the fabricated device (b) 3.5cm ×2cm and (c) 3.5cm ×1cm.

3.3. Sensor Characterization

Sensors were observed under optical microscope at different resolutions using Olympus BX51M computerized HR digital colored microscope. The surface morphology and film thickness of the sensors was measured by cross sectional SEM using Jeol JSM-7600F Scanning Electron

Microscope. 2D and 3D surface profiles of the films were obtained by Nano View high accuracy non-contact surface profiler.

The sensors' electrical response was measured using Applent AT825 digital LCR Meter and by connecting it to computer for data logging and processing. The measurement setup and schematic for measuring the bending angles response is shown in Figure 3-4.

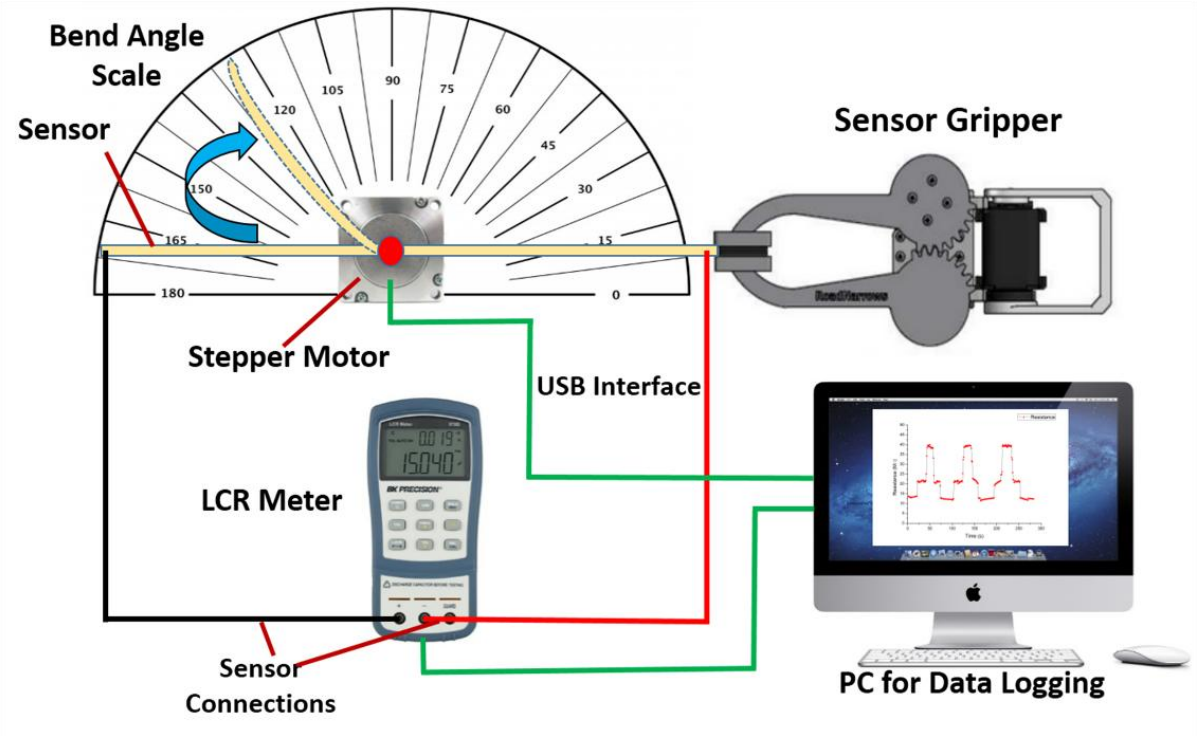

Figure 3-4: The schematic diagram of the setup used for measuring bending angles response of the sensors.

3.4. Results and Discussion

The sensors with $ZnSnO_3$/PVDF composite film were observed under optical microscope to observe the high resolution images of the fabricated films and to inspect the quality of deposition. The images are shown in Figure 3-5.

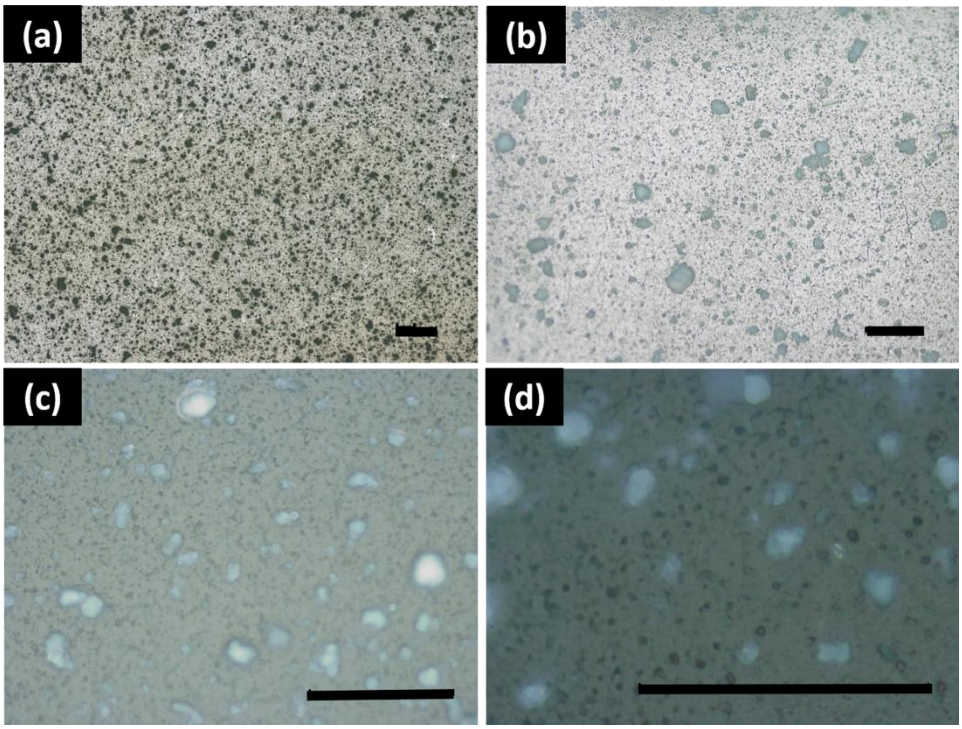

Figure 3-5: Microscopic images of the PET substrate coated with $ZnSnO_3$/PVDF composite film at different magnifications (X) (a) PET coated with $ZnSnO_3$/PVDF film (5X) ;scale = 200µm, (b) PET coated with $ZnSnO_3$/PVDF film (20X) ;scale = 100µm, (c) PET coated with $ZnSnO_3$/PVDF film (50X) ;scale = 100µm, (d) PET coated with $ZnSnO_3$/PVDF film (100X) ;scale = 100µm.

The 2D and 3D surface profiles of the coated film were obtained to visualize the surface morphology of the films. The roughness in the surface area of the films is due to the presence of $ZnSnO_3$ nanocubes, which gives high mobility for large range of bending angles i.e -150° to 0° to 150°.

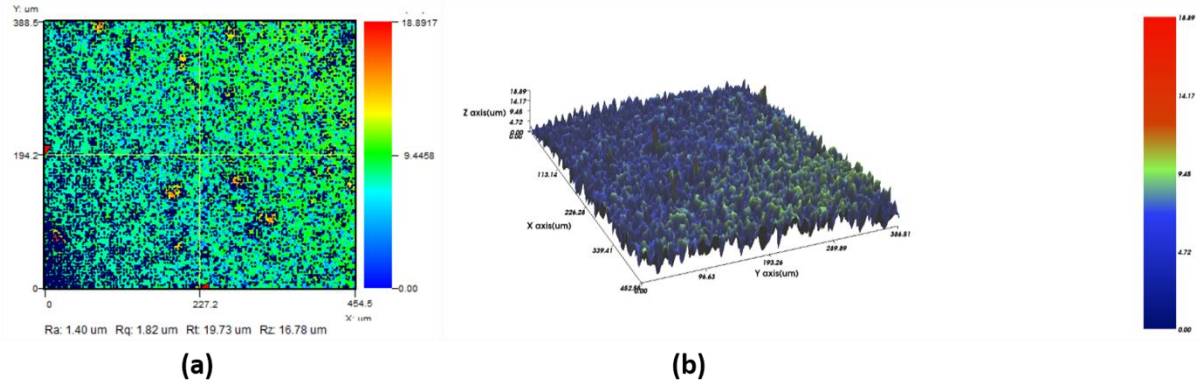

Figure 3-6: 2D and 3D Surface profiles of the $ZnSnO_3$/PVDF film (a) 2D profile and (b) 3D profile.

Optical microscopy confirmed the quality of deposition of the films over a large area of view. Surface electron microscopy was performed for both the surface profile and the cross-sectional view. The SEM images are shown in Figure 3-7.

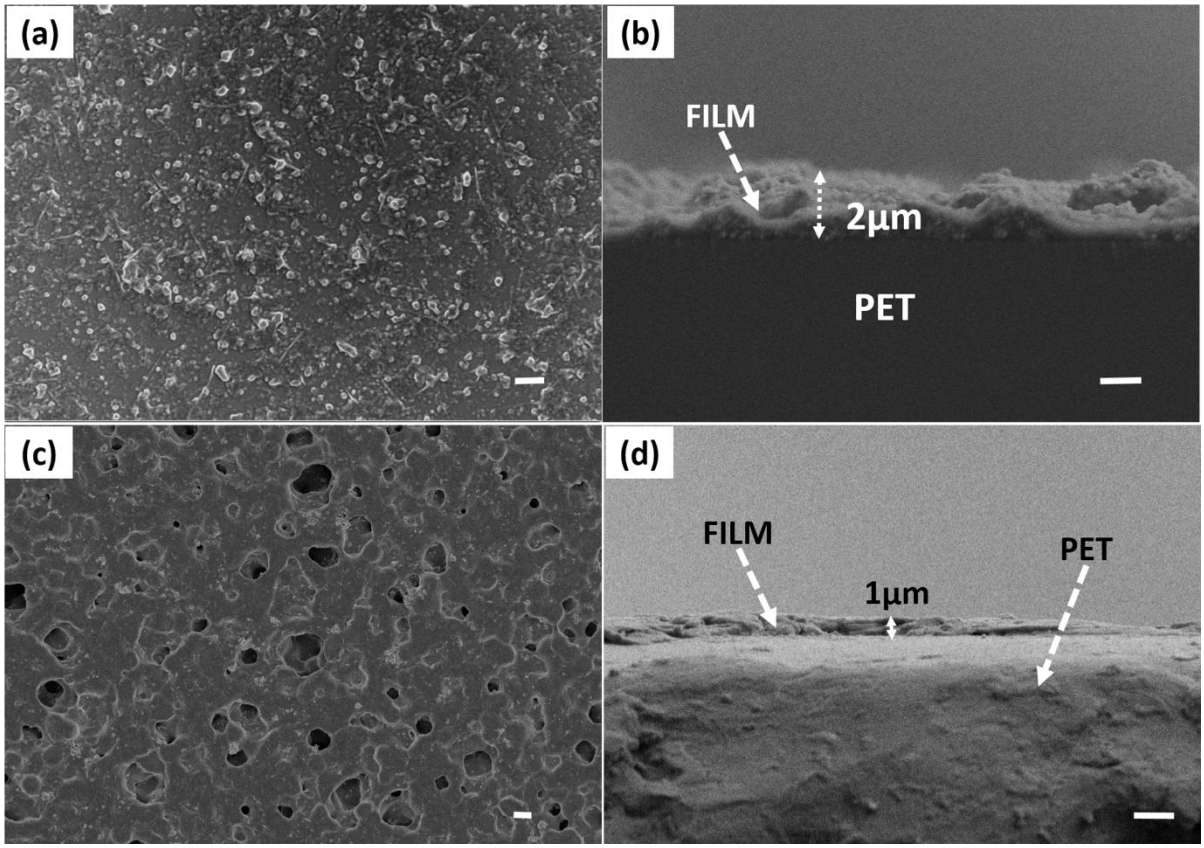

Figure 3-7: SEM images of the fabricated films. (a) Surface SEM of the $ZnSnO_3$/PVDF film, (b) Cross-sectional SEM image of the film ,scale bar = 1µm, (c) Surface SEM of the $ZnSnO_3$/PVDF film, scale bar = 500nm (d) Cross-sectional SEM image of the film, scale bar = 2µm.

The surface profile results shown in Figure 3-7(a) clearly indicate that the surface finish of the composite film is highly rough due to the presence of $ZnSnO_3$ nanocubes. The high surface roughness indicates loosely arranged particles in the film displaying room for their mechanical movement on the application of external force on the sensing layer through bending at different angles. The movement of particles by application of force improves the connection between them when the sensor is bent in negative direction thus reducing the device resistance and vice versa. The cross-sectional SEM images presented in Figure 3-7(b and d) indicate the thickness of the

active layer is ~2µm and ~1µm. Sensors response for both film thickness has been presented in Figure 3-8 (a and b), which is in accordance with the general principle of thin films resistance, that the resistance increases with decreasing film thickness and vice versa.

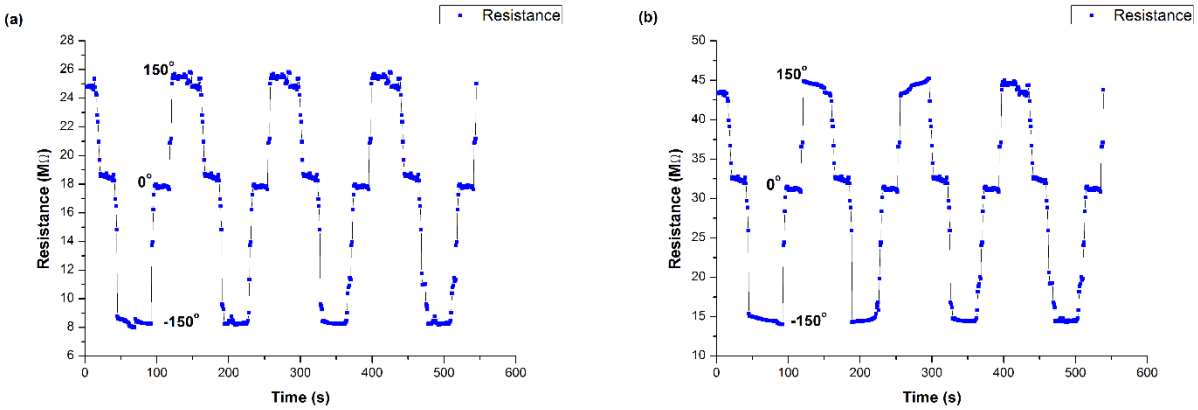

Figure 3-8: Resistance response of sensors of different thicknesses (a) 2µm and (b) 1µm

Two different flex sensors were fabricated with varying dimensions to investigate the effect of size on the electrical properties. The resistance of the fabricated flex sensors depends upon the physical properties like length, width, and bend angle etc. The change in resistance of the different sensors was measured with respect to the bend angle and width. Two sensors with different widths were tested and their electrical response was recorded. The response of the sensors with different dimensions was then compared. Figure 3-9 and Figure 3-10 show the graphs of the sensors comparing different dimensions.

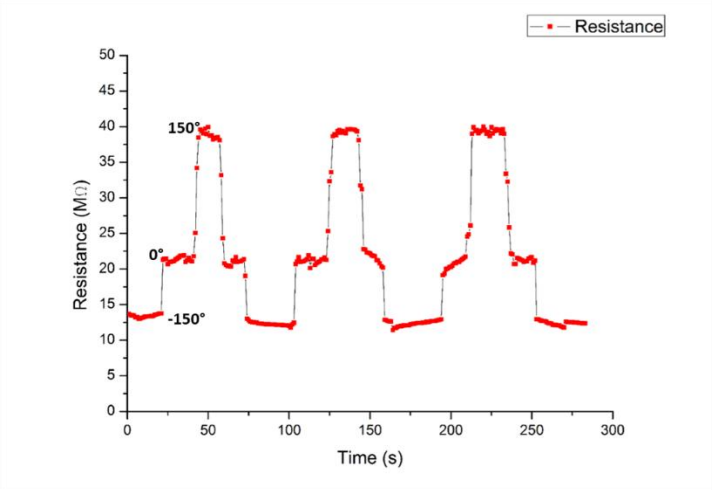

Figure 3-9: Sensor response with 3.5cm ×2cm sensor dimensions for bending angles of -150° to 0° to 150°.

As can be seen in Figure 3-9, the resistance of the sensor with dimensions 3.5cm ×2cm, is quite high, range of 10's of Mega-Ohms and switches stably between ~15MΩ to ~40 MΩ for -150° to 0° to 150° bend angles respectively. Also, the resistance switches between ~20MΩ to ~100 MΩ for -150° to 0° to 150° bend angles respectively for the sensors with dimensions 3.5cm ×1cm. Figure 3-10 shows the response of the sensors with dimensions 3.5cm ×1cm.

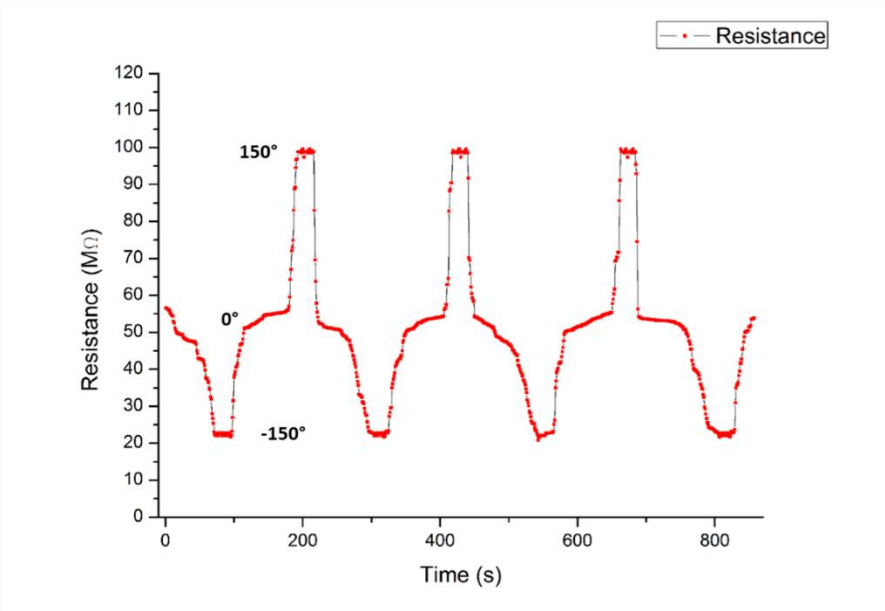

Figure 3-10: Sensor response with 3.5cm ×1cm sensor dimensions for bending angles of -150° to 0° to 150°.

This behavior clearly shows the effect of width on the sensor's resistance. The smaller the width, the lower the overall resistance of the sensor.

Sensors were tested for durability for multiple number of bend cycles. Resistance response of the sensors was plotted after 0 cycles, 500 cycles, and 1000 cycles to see the change in resistance of the sensors due to possible micro defects from bending. The data plots are presented in Figure 3-11.

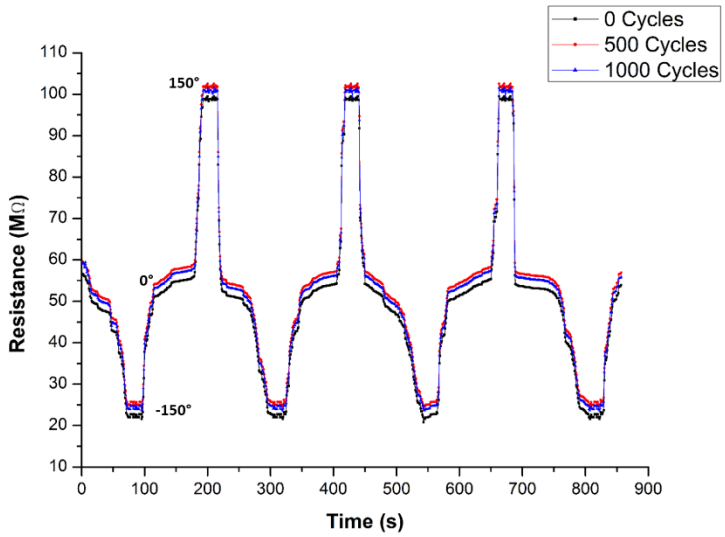

Figure 3-11: Durability test of sensor with dimensions 3.5cm ×1cm after bending at different number of cycles.

The plots clearly show that the sensors are highly stable and durable up to 1000 cycles.

The highly stable sensors operation is achieved through the addition of PVDF as a binding agent in zinc stannate that prevents cracking and other permanent mechanical deformations in the active layer.

4. Conclusions and Future Prospects

4.1. Conclusions

The main goal of this project was to fabricate and characterize low cost printed sensors which can be used for environment and health monitoring with fast response and recovery time. This goal has been achieved, since different kind of sensors were created using commercially available printing materials, and unique printing systems. The key conclusions of the research work can be summarized as:

1. A new nano-composite sensing material (PEDOT:PSS and $ZnSnO_3$) has been developed for relative humidity sensing which is capable of sensing a wide range of relative humidity (0%-90%), with high stability, repeatability, and fast response and recovery times with linear impedance response.

2. A water assisted transfer method for the fabrication of Micro/nano devices has been studied to fabricate (PEDOT:PSS and $ZnSnO_3$) based humidity sensor, owing to its low cost, simple fabrication technique, efficient performance, and robustness in bendability, and conformability onto a wide range of smooth and highly rough arbitrary substrates. Moreover, the device demonstrates the flexibility down to mm scale radius of curvature. The transferring technique can be utilized for developing layer by layer structures, which have high potential in the applications like flexible sensors, flexible display devices, skin mounted devices, and environmental sensors.

3. Moreover we have fabricated $ZnSnO_3$/PVDF thin films and used this structure as a body motion sensor for measuring minor changes in body motion. The dielectric behavior of PVDF has improved owing to the piezoelectric barrier provided by the $ZnSnO_3$ nanocubes. The β-Phase PVDF and octahedral structure of $ZnSnO_3$ have shown high change in electrical resistance via the piezoresistance of the material, which will be helpful in the detection of minor movements for

artificial skin applications. The durability tests show that the sensor is durable for at least upto 1000 bending cycles.

4.2. Future Prospects

The research work presented in this thesis has showed promising results. However there were number of technical issues observed during the development of printed sensors. Such issues are important enough to be discussed for future studies to improve the results.

Due to time constraints, the stability of the humidity sensors over time was not investigated. This is clearly one aspect of the humidity sensor construction that would need to be investigated. It is important because humidity sensors must have a shelf-life of months for their production and proven to be economically viable.

This study used various substrates ranging from rigid substrates like glass, silicon etc., flexible substrates like PET, and arbitrary shaped substrates like plant leaves and animal shells, for printing sensors. Finally, it would be interesting to use non-vacuum printing techniques to fabricate sensors on stretchable substrates for health monitoring, and skin mounted sensor applications.

References

[1] H. Bai, G. Shi, Gas Sensors Based on Conducting Polymers, Sensors. 7 (2007) 267–307. doi:10.3390/s7030267.

[2] M.T.S. Chani, K.S.S. Karimov, F.A. Khalid, S.A. Moiz, Polyaniline based impedance humidity sensors, Solid State Sci. 18 (2013) 78–82. doi:10.1016/j.solidstatesciences.2013.01.005.

[3] A. Sun, Z. Li, T. Wei, Y. Li, P. Cui, Highly sensitive humidity sensor at low humidity based on the quaternized polypyrrole composite film, Sensors Actuators B Chem. 142 (2009) 197–203. doi:10.1016/j.snb.2009.08.028.

[4] S. Taccola, F. Greco, A. Zucca, C. Innocenti, C. De Julián Fernández, G. Campo, et al., Characterization of free-standing PEDOT:PSS/iron oxide nanoparticle composite thin films and application as conformable humidity sensors, ACS Appl. Mater. Interfaces. 5 (2013) 6324–6332. doi:10.1021/am4013775.

[5] R. Singh, Synthesis and Humidity Sensing Investigations of Nanostructured $ZnSnO_3$, J. Sens. Technol. 1 (2011) 116–124. doi:10.4236/jst.2011.14016.

[6] U. Mogera, A. a Sagade, S.J. George, G.U. Kulkarni, Ultrafast response humidity sensor using supramolecular nanofibre and its application in monitoring breath humidity and flow., Sci. Rep. 4 (2014) 4103. doi:10.1038/srep04103.

[7] Y. Li, M.J. Yang, Y. Chen, Nanocomposites of carbon nanotubes and silicone-containing polyelectrolyte as a candidate for construction of humidity sensor, J. Mater. Sci. 40 (2005) 245–247. doi:10.1007/s10853-005-5719-9.

[8] K. Jaruwongrungsee, C. Sriprachuabwong, A. Sappat, A. Wisitsoraat, P. Phasukkit, M. Sangworasil, et al., High-sensitivity humidity sensor utilizing PEDOT/PSS printed quartz crystal microbalance, 8th Electr. Eng. Electron. Comput. Telecommun. Inf. Technol. Assoc. Thail. - Conf. 2011. (2011) 66–69. doi:10.1109/ECTICON.2011.5947772.

[9] Y. Chen, L. Yu, Q.Q.Q.Q. Li, Y. Wu, Q.Q.Q.Q. Li, T. Wang, Nanosheets With Excellent Gas Sensing Performance, Nanotechnology. 23 (2012) 415501. doi:10.1088/0957-4484/23/41/415501.

[10] P. Song, Q. Wang, Z. Yang, Biomorphic synthesis of ZnSnO3 hollow fibers for gas sensing application, Sensors Actuators B Chem. 156 (2011) 983–989. doi:10.1016/j.snb.2011.03.017.

[11] C. Wang, L. Yin, L. Zhang, D. Xiang, R. Gao, Metal oxide gas sensors: Sensitivity and influencing factors, Sensors. 10 (2010) 2088–2106. doi:10.3390/s100302088.

[12] I. Stambolova, K. Konstantinov, D. Kovacheva, P. Peshev, T. Donchev, Spray Pyrolysis Preparation and Humidity Sensing Characteristics of Spinel Zinc Stannate Thin Films, J. Solid State Chem. 128 (1997) 305–309. doi:10.1006/jssc.1996.7174.

[13] N.D. Md Sin, M.H. Mamat, M.F. Malek, M. Rusop, Fabrication of nanocubic ZnO/SnO2 film-based humidity sensor with high sensitivity by ultrasonic-assisted solution growth method at different Zn:Sn precursor ratios, Appl. Nanosci. 4 (2013) 829–838. doi:10.1007/s13204-013-0262-5.

[14] J. Jian, X. Guo, L. Lin, Q. Cai, J. Cheng, J. Li, Gas-sensing characteristics of dielectrophoretically assembled composite film of oxygen plasma-treated SWCNTs and PEDOT/PSS polymer, Sensors Actuators B Chem. 178 (2013) 279–288.

doi:10.1016/j.snb.2012.12.085.

[15] G. Zhang, C. Xie, A novel method in the gas identification by using WO3 gas sensor based on the temperature-programmed technique, Sensors Actuators B Chem. 206 (2015) 220–229. doi:10.1016/j.snb.2014.09.063.

[16] a. Sappat, a. Wisitsoraat, C. Sriprachuabwong, K. Jaruwongrungsee, T. Lomas, a. Tuantranont, Humidity sensor based on piezoresistive microcantilever with inkjet printed PEDOT/PSS sensing layers, 8th Electr. Eng. Electron. Comput. Telecommun. Inf. Technol. Assoc. Thail. - Conf. 2011. (2011) 34–37. doi:10.1109/ECTICON.2011.5947764.

[17] M. Kuş, S. Okur, Electrical characterization of PEDOT:PSS beyond humidity saturation, Sensors Actuators B Chem. 143 (2009) 177–181. doi:10.1016/j.snb.2009.08.055.

[18] C.H. Lee, W.Y. Chuang, S.H. Lin, W.J. Wu, C.T. Lin, A Printable humidity sensing material based on conductive polymer and nanoparticles composites, Jpn. J. Appl. Phys. 52 (2013). doi:10.7567/JJAP.52.05DA08.

[19] C.-H. Lee, W.-Y. Chuang, M. Cowan, W.-J. Wu, C.-T. Lin, A Low-Power Integrated Humidity CMOS Sensor by Printing-on-Chip Technology, Sensors. 14 (2014) 9247–9255. doi:10.3390/s140509247.

[20] S. Borini, R. White, D. Wei, M. Astley, S. Haque, E. Spigone, et al., Ultrafast graphene oxide humidity sensors., ACS Nano. 7 (2013) 11166–73. doi:10.1021/nn404889b.

[21] Y. Li, L. Hong, Y. Chen, H. Wang, X. Lu, M. Yang, Poly(4-vinylpyridine)/carbon black composite as a humidity sensor, Sensors Actuators, B Chem. 123 (2007) 554–559.

doi:10.1016/j.snb.2006.09.057.

[22] K. Jiang, T. Fei, F. Jiang, G. Wang, T. Zhang, A dew sensor based on modified carbon black and polyvinyl alcohol composites, Sensors Actuators, B Chem. 192 (2014) 658–663. doi:10.1016/j.snb.2013.11.004.

[23] N.D. Md Sin, N. Khadijah, M.H. Mamat, M.Z. Musa, M. Rusop Mahmood, Influence of Cubic Structured-$ZnSnO_3$ Immersion Time to the Performance of Humidity Sensor, Nano Hybrids. 2 (2012) 1–11. doi:10.4028/www.scientific.net/NH.2.1.

[24] Z. Ahmad, Q. Zafar, K. Sulaiman, R. Akram, K.S. Karimov, A humidity sensing organic-inorganic composite for environmental monitoring., Sensors (Basel). 13 (2013) 3615–24. doi:10.3390/s130303615.

[25] K.H. Choi, M. Sajid, S. Aziz, B.-S. Yang, Wide range high speed relative humidity sensor based on PEDOT:PSS–PVA composite on an IDT printed on piezoelectric substrate, Sensors Actuators A Phys. 228 (2015) 40–49. doi:10.1016/j.sna.2015.03.003.

[26] K.H. Choi, G.U. Siddiqui, B. Yang, M. Mustafa, Synthesis of ZnSnO3 nanocubes and thin film fabrication of (ZnSnO3/PMMA) composite through electrospray deposition, J. Mater. Sci. Mater. Electron. (2015). doi:10.1007/s10854-015-3121-1.

[27] C. Gao, J. Li, J. Liu, J. Zhang, H. Sun, Influence of MWCNTs doping on the structure and properties of PEDOT:PSS films, Int. J. Photoenergy. 2009 (2009) 1–5. doi:10.1155/2009/650509.

[28] Z. Chen, C. Lu, Humidity Sensors: A Review of Materials and Mechanisms, Sens. Lett. 3 (2005) 274–295. doi:10.1166/sl.2005.045.

[29] J. Boyle, The effects of CO, water vapor and surface temperature on the conductivity of a SnO 2 gas sensor, J. Electron. Mater. 6 (1977) 717–733. http://www.springerlink.com/index/U172876214G24600.pdf.

[30] Y. Chen, L. Yu, Q. Li, Y. Wu, Q. Li, T. Wang, An evolution from 3D face-centered-cubic ZnSnO3 nanocubes to 2D orthorhombic ZnSnO3 nanosheets with excellent gas sensing performance., Nanotechnology. 23 (2012) 415501. doi:10.1088/0957-4484/23/41/415501.

[31] D. Han, G. Yang, J. Song, L. Niu, A. Ivaska, Morphology of electrodeposited poly(3,4-ethylenedioxythiophene)/poly(4-styrene sulfonate) films, J. Electroanal. Chem. 602 (2007) 24–28. doi:10.1016/j.jelechem.2006.11.027.

[32] M. Deepa, a. K. Srivastava, K.N. Sood, a. V. Murugan, Nanostructured Tungsten Oxide-Poly(3,4-ethylenedioxythiophene):Poly(styrenesulfonate) Hybrid Films: Synthesis, Electrochromic Response, and Durability Characteristics, J. Electrochem. Soc. 155 (2008) D703. doi:10.1149/1.2975388.

[33] E. Sheha, M. Nasr, M.K. El-Mansy, Characterization of poly (vinyl alcohol)/poly(3,4-ethylenedioxythiophene) poly(styrenesulfonate) polymer blend: structure, optical absorption, electrical and dielectric properties, Phys. Scr. 88 (2013) 35701. doi:10.1088/0031-8949/88/03/035701.

[34] J. Ju, Y. Yamagata, H. Ohmori, T. Higuchi, High-frequency surface acoustic wave atomizer, Sensors Actuators, A Phys. 145–146 (2008) 437–441. doi:10.1016/j.sna.2008.01.001.

[35] M.S. Gong, M.H. Lee, H.W. Rhee, Humidity sensor using cross-linked copolymers

containing viologen moiety, Sensors Actuators, B Chem. 73 (2001) 185–191.

[36] K.P. Yoo, L.T. Lim, N.K. Min, M.J. Lee, C.J. Lee, C.W. Park, Novel resistive-type humidity sensor based on multiwall carbon nanotube/polyimide composite films, Sensors Actuators, B Chem. 145 (2010) 120–125. doi:10.1016/j.snb.2009.11.041.

[37] S.K. Mahadeva, S. Yun, J. Kim, Flexible humidity and temperature sensor based on cellulose-polypyrrole nanocomposite, Sensors Actuators, A Phys. 165 (2011) 194–199. doi:10.1016/j.sna.2010.10.018.

[38] K. Ogura, T. Saino, M. Nakayama, H. Shiigi, The humidity dependence of the electrical conductivity of a soluble polyaniline – poly (vinyl alcohol) composite film, 7 (1997) 2363–2366.

[39] A.C. Power, A.J. Betts, J.F. Cassidy, Silver nanoparticle polymer composite based humidity sensor., Analyst. 135 (2010) 1645–52. doi:10.1039/c0an00133c.

[40] R.P. Singh, M. Joshi, POLYMER - INORGANIC NANOPARTICLE COMPOSITES FOR HUMIDITY SENSOR, (n.d.) 3–4.

[41] Y. Li, M.J. Yang, Y. She, Humidity sensitive properties of crosslinked and quaternized poly(4-vinylpyridine-co-butyl methacrylate), Sensors Actuators B Chem. 107 (2005) 252–257. doi:10.1016/j.snb.2004.10.008.

[42] M.T.S. Chani, K.S. Karimov, F.A. Khalid, S.A. Moiz, Polyaniline based impedance humidity sensors, Solid State Sci. 18 (2013) 78–82. doi:10.1016/j.solidstatesciences.2013.01.005.

[43] W. a. Daoud, J.H. Xin, Y.S. Szeto, Polyethylenedioxythiophene coatings for humidity,

temperature and strain sensing polyamide fibers, Sensors Actuators B Chem. 109 (2005) 329–333. doi:10.1016/j.snb.2004.12.067.

[44] G. Campo, C. Sangregorio, B. Mazzolai, V. Mattoli, Characterization of Free-Standing PEDOT:PSS/Iron Oxide Nanoparticle Composite Thin Films and Application As Conformable Humidity Sensors, (2013).

[45] C.H. Lee, J.-H. Kim, C. Zou, I.S. Cho, J.M. Weisse, W. Nemeth, et al., Peel-and-stick: mechanism study for efficient fabrication of flexible/transparent thin-film electronics., Sci. Rep. 3 (2013) 2917. doi:10.1038/srep02917.

[46] C.H. Lee, D.R. Kim, I.S. Cho, N. William, Q. Wang, X. Zheng, Peel-and-stick: fabricating thin film solar cell on universal substrates., Sci. Rep. 2 (2012) 1000. doi:10.1038/srep01000.

[47] C. Dagdeviren, Y. Su, P. Joe, R. Yona, Y. Liu, Y.-S. Kim, et al., Conformable amplified lead zirconate titanate sensors with enhanced piezoelectric response for cutaneous pressure monitoring., Nat. Commun. 5 (2014) 4496. doi:10.1038/ncomms5496.

[48] J. Yoon, A.J. Baca, S.-I. Park, P. Elvikis, J.B. Geddes, L. Li, et al., Ultrathin silicon solar microcells for semitransparent, mechanically flexible and microconcentrator module designs., Nat. Mater. 7 (2008) 907–15. doi:10.1038/nmat2287.

[49] M. a. Meitl, Z.-T. Zhu, V. Kumar, K.J. Lee, X. Feng, Y.Y. Huang, et al., Transfer printing by kinetic control of adhesion to an elastomeric stamp, Nat. Mater. 5 (2005) 33–38. doi:10.1038/nmat1532.

[50] L. Faculty, R. John, Micro-Transfer Printing - Flexible and Stretchable Electronics, (n.d.).

[51] S.C.B. Mannsfeld, B.C.-K. Tee, R.M. Stoltenberg, C.V.H.-H. Chen, S. Barman, B.V.O. Muir, et al., Highly sensitive flexible pressure sensors with microstructured rubber dielectric layers., Nat. Mater. 9 (2010) 859–64. doi:10.1038/nmat2834.

[52] C.H. Lee, D.R. Kim, X. Zheng, Fabrication of nanowire electronics on nonconventional substrates by water-assisted transfer printing method., Nano Lett. 11 (2011) 3435–9. doi:10.1021/nl201901z.

[53] W. Deng, X. Zhang, H. Pan, Q. Shang, J. Wang, X. Zhang, et al., A High-yield Two-step Transfer Printing Method for Large-scale Fabrication of Organic Single-crystal Devices on Arbitrary Substrates., Sci. Rep. 4 (2014) 5358. doi:10.1038/srep05358.

[54] Y. Zhang, J.J. Magan, W.J. Blau, A general strategy for hybrid thin film fabrication and transfer onto arbitrary substrates., Sci. Rep. 4 (2014) 4822. doi:10.1038/srep04822.

[55] M. Ikawa, T. Yamada, H. Matsui, H. Minemawari, J. Tsutsumi, Y. Horii, et al., Simple push coating of polymer thin-film transistors., Nat. Commun. 3 (2012) 1176. doi:10.1038/ncomms2190.

[56] H.H. Kim, Y. Chung, E. Lee, S.K. Lee, K. Cho, Water-free transfer method for CVD-grown graphene and its application to flexible air-stable graphene transistors., Adv. Mater. 26 (2014) 3213–7. doi:10.1002/adma.201305940.

[57] J. Jeong, J. Kim, K. Song, K. Autumn, J. Lee, Geckoprinting: assembly of microelectronic devices on unconventional surfaces by transfer printing with isolated gecko setal arrays., J. R. Soc. Interface. 11 (2014). doi:10.1098/rsif.2014.0627.

[58] Y. Kobayashi, K. Kumakura, T. Akasaka, T. Makimoto, Layered boron nitride as a

release layer for mechanical transfer of GaN-based devices, Nature. 484 (2012) 223–227. doi:10.1038/nature10970.

[59] V.K. Sangwan, a. Southard, T.L. Moore, V.W. Ballarotto, D.R. Hines, M.S. Fuhrer, et al., Transfer printing approach to all-carbon nanoelectronics, Microelectron. Eng. 88 (2011) 3150–3154. doi:10.1016/j.mee.2011.06.017.

[60] Q.N. Thanh, H. Jeong, J. Kim, J.W. Kevek, Y.H. Ahn, S. Lee, et al., Transfer-printing of as-fabricated carbon nanotube devices onto various substrates, Adv. Mater. 24 (2012) 4499–4504. doi:10.1002/adma.201201794.

[61] M. Kaltenbrunner, T. Sekitani, J. Reeder, T. Yokota, K. Kuribara, T. Tokuhara, et al., An ultra-lightweight design for imperceptible plastic electronics., Nature. 499 (2013) 458–63. doi:10.1038/nature12314.

[62] J.M. Weisse, C.H. Lee, D.R. Kim, X. Zheng, Fabrication of flexible and vertical silicon nanowire electronics., Nano Lett. 12 (2012) 3339–43. doi:10.1021/nl301659m.

[63] S. Kim, J.H. Son, S.H. Lee, B.K. You, K.-I. Park, H.K. Lee, et al., Flexible Crossbar-Structured Resistive Memory Arrays on Plastic Substrates via Inorganic-Based Laser Lift-Off, Adv. Mater. (2014) 7480–7487. doi:10.1002/adma.201402472.

[64] N. Li, X. Chen, X. Chen, X. Ding, X. Li, Subsecond Response of Humidity Sensor Based on Graphene Oxide Quantum Dots, Ieee Electron Device Lett. 36 (2015) 615–617.

[65] C.L. Cao, C.G. Hu, L. Fang, S.X. Wang, Y.S. Tian, C.Y. Pan, Humidity sensor based on multi-walled carbon nanotube thin films, J. Nanomater. 2011 (2011). doi:10.1155/2011/707303.

[66] Q. Qi, T. Zhang, Q. Yu, R. Wang, Y. Zeng, L. Liu, et al., Properties of humidity sensing ZnO nanorods-base sensor fabricated by screen-printing, Sensors Actuators, B Chem. 133 (2008) 638–643. doi:10.1016/j.snb.2008.03.035.

[67] P.K. Kannan, R. Saraswathi, J.B.B. Rayappan, A highly sensitive humidity sensor based on DC reactive magnetron sputtered zinc oxide thin film, Sensors Actuators, A Phys. 164 (2010) 8–14. doi:10.1016/j.sna.2010.09.006.

[68] S.K. Mahadeva, S. Yun, J. Kim, Flexible humidity and temperature sensor based on cellulose–polypyrrole nanocomposite, Sensors Actuators A Phys. 165 (2011) 194–199. doi:10.1016/j.sna.2010.10.018.

[69] S.M. Mehdi, J. Jo, Y.H. Doh, H.W. Dang, K.H. Choi, Stretchable and flexible resistive behavior of poly(3,4-ethylenedioxythiophene):Poly(styrenesulfonate) thin film on ultra-low modulus polydimethylsiloxane with trench-type roughness, J. Polym. Sci. Part B Polym. Phys. 53 (2015) 226–233. doi:10.1002/polb.23615.

[70] M. Mehdi, K.H. Cho, K.H. Choi, Versatile poly(3,4-ethylenedioxythiophene) poly(styrenesulfonate) films on polydimethylsiloxane substrates having random micro ridges: Study of resistive behaviors of a polymer-polymer laminate, J. Appl. Polym. Sci. 41235 (2014) 1–6. doi:10.1002/app.41235.

[71] S.M. Mehdi, K.H. Cho, K.H. Choi, Stretchability and resistive behavior of silver (Ag) nanoparticle films on polydimethylsiloxane (PDMS) with random micro ridges, J. Mater. Sci. Mater. Electron. 25 (2014) 3375–3382. doi:10.1007/s10854-014-2028-6.

[72] S. Aziz, D.E. Chang, Y.H. Doh, C.U. Kang, K.H. Choi, Humidity Sensor Based on PEDOT:PSS and Zinc Stannate Nano-composite, J. Electron. Mater. 44 (2015) 3992–

3999. doi:10.1007/s11664-015-3914-2.

[73] S.M. Mehdi, K.H. Cho, C.N. Kang, K.H. Choi, Stretchability of Silver Films on Thin Acid-Etched Rough Polydimethylsiloxane Substrates Fabricated by Electrospray Deposition, J. Electron. Mater. 44 (2015) 2514–2521. doi:10.1007/s11664-015-3813-6.

[74] D.R. Hines, V.W. Ballarotto, E.D. Williams, Y. Shao, S. a. Solin, Transfer printing methods for the fabrication of flexible organic electronics, J. Appl. Phys. 101 (2007) 24503. doi:10.1063/1.2403836.

[75] F.N. Ishikawa, H.K. Chang, K. Ryu, P.C. Chen, A. Badmaev, L.G. De Arco, et al., Transparent electronics based on transfer printed aligned carbon nanotubes on rigid and flexible substrates, ACS Nano. (2009). doi:10.1021/nn800434d.

[76] D.Y. Lee, D.R. Hines, C.M. Stafford, C.L. Soles, E.K. Lin, G.S. Oehrlein, Low-temperature plasma-assisted nanotransfer printing between thermoplastic polymers, Adv. Mater. 21 (2009) 2524–2529. doi:10.1002/adma.200803121.

[77] S. Kim, J. Wu, A. Carlson, S.H. Jin, A. Kovalsky, P. Glass, et al., Microstructured elastomeric surfaces with reversible adhesion and examples of their use in deterministic assembly by transfer printing., Proc. Natl. Acad. Sci. U. S. A. 107 (2010) 17095–17100. doi:10.1073/pnas.1005828107.

[78] C.H. Lee, D.R. Kim, X. Zheng, Fabricating nanowire devices on diverse substrates by simple transfer-printing methods., Proc. Natl. Acad. Sci. U. S. A. 107 (2010) 9950–5. doi:10.1073/pnas.0914031107.

[79] M.L. Tseng, B.H. Chen, C.H. Chu, C.M. Chang, W.C. Lin, N.-N. Chu, et al., Fabrication

of phase-change chalcogenide Ge_2Sb_2Te_5 patterns by laser-induced forward transfer, Opt. Express. 19 (2011) 16975. doi:10.1364/OE.19.016975.

[80] G. a Salvatore, N. Münzenrieder, T. Kinkeldei, L. Petti, C. Zysset, I. Strebel, et al., Wafer-scale design of lightweight and transparent electronics that wraps around hairs., Nat. Commun. 5 (2014) 2982. doi:10.1038/ncomms3982.

[81] L.G.P. Martins, Y. Song, T. Zeng, M.S. Dresselhaus, J. Kong, P.T. Araujo, Direct transfer of graphene onto flexible substrates., Proc. Natl. Acad. Sci. U. S. A. 110 (2013) 17762–7. doi:10.1073/pnas.1306508110.

[82] W.-H. Yeo, Y.-S. Kim, J. Lee, A. Ameen, L. Shi, M. Li, et al., Multifunctional epidermal electronics printed directly onto the skin., Adv. Mater. 25 (2013) 2773–8. doi:10.1002/adma.201204426.

[83] H. Cho, S. Somu, J.Y. Lee, H. Jeong, A. Busnaina, High-Rate Nanoscale Offset Printing Process Using Directed Assembly and Transfer of Nanomaterials, Adv. Mater. (2015) n/a-n/a. doi:10.1002/adma.201404769.

[84] M.K. Choi, J. Yang, K. Kang, D.C. Kim, C. Choi, C. Park, et al., Wearable red–green–blue quantum dot light-emitting diode array using high-resolution intaglio transfer printing, Nat. Commun. 6 (2015) 7149. doi:10.1038/ncomms8149.

[85] J. Liang, L. Li, D. Chen, T. Hajagos, Z. Ren, S.-Y. Chou, et al., Intrinsically stretchable and transparent thin-film transistors based on printable silver nanowires, carbon nanotubes and an elastomeric dielectric, Nat. Commun. 6 (2015) 7647. doi:10.1038/ncomms8647.

[86] M. Melzer, D. Karnaushenko, G. Lin, S. Baunack, D. Makarov, O.G. Schmidt, Direct

Transfer of Magnetic Sensor Devices to Elastomeric Supports for Stretchable Electronics, Adv. Mater. 27 (2015) 1333–1338. doi:10.1002/adma.201403998.

[87] H. Liu, W. Sun, S. Xu, An extremely simple thermocouple made of a single layer of metal, Adv. Mater. 24 (2012) 3275–3279. doi:10.1002/adma.201200644.

[88] S. Micro, N.P. Nanogenerators, S.T. Sensors, Single Micro / Nanowire Pyroelectric, ACS Nano. 6 (2012) 8456–8461. doi:10.1021/nn303414u.

[89] C.G. Haugh, J.E. Marcy, J.H. Wilson, F.A. Agblevor, A Thermistor Based Method for Measurement of Thermal Conductivity and Thermal Diffusivity of Moist Food Materials at High Temperatures, (1998).

[90] S. Sahoo, S.K.S. Parashar, S.M. Ali, CaTiO 3 nano ceramic for NTCR thermistor based sensor application, J. Adv. Ceram. 3 (2014) 117–124. doi:10.1007/s40145-014-0100-6.

[91] R. Strümpler, R. Stru, Polymer composite thermistors for temperature and current sensors Polymer composite thermistors for temperature and current sensors, J. Appl. Phys. 6091 (1997). doi:10.1063/1.363682.

[92] S. Ryu, I. Yoo, S. Song, B. Yoon, J. Kim, A Thermoresponsive Fluorogenic Conjugated Polymer for a Temperature Sensor in Microfluidic Devices A Thermoresponsive Fluorogenic Conjugated Polymer for a Temperature Sensor in Microfluidic Devices, JACS. (2009) 3800–3801. doi:10.1021/ja808077d.

[93] J. Jeon, H.-B.-R. Lee, Z. Bao, Flexible wireless temperature sensors based on Ni microparticle-filled binary polymer composites., Adv. Mater. 25 (2013) 850–5. doi:10.1002/adma.201204082.

[94] X. Ren, P.K.L. Chan, J. Lu, B. Huang, D.C.W. Leung, High dynamic range organic temperature sensor., Adv. Mater. 25 (2013) 1291–5. doi:10.1002/adma.201204396.

[95] S. Harada, W. Honda, T. Arie, S. Akita, K. Takei, Fully Printed , Highly Sensitive Multifunctional Arti fi cial Electronic Whisker Arrays Integrated with Strain and Temperature Sensors, ACS Nano. 8 (2014) 3921–3927. doi:10.1021/nn500845a.

[96] P. Kumar, J. Verma, S. Prasad, Hand Data Glove: A Wearable Real-Time Device for Human-Computer Interaction, Int. J. Adv. Sci. Technol. 43 (2012) 15–26.

[97] N.H. Adnan, K. Wan, S. Ab, S. Khadijah, H. Desa, M. Azri, et al., The Development of a Low Cost Data Glove by Using Flexible Bend Sensor for Resistive Interfaces, 2012 (2012) 579–587.

[98] S.K. Dixit, N.S. Shingi, Implementation of Flex sensor and Electronic Compass for Hand Gesture Based Wireless Automation of Material, 2 (2012) 2–4.

[99] N.H. Adnan, K. Wan, a. B. Shahriman, M.H. Ali, M. Nasir Ayob, A. a. Aziz, Development of low cost “GloveMAP” based on fingertip bending tracking techniques for virtual interaction, Int. J. Mech. Mechatronics Eng. 12 (2012) 41–51.

[100] N. Tongrod, T. Kerdcharoen, N. Watthanawisuth, A. Tuantranont, A low-cost data-glove for Human computer interaction based on ink-jet printed sensors and ZigBee networks, Int. Symp. Wearable Comput. 2010. (2010) 1–2. doi:10.1109/ISWC.2010.5665850.

[101] A. Raut, V. Singh, V. Rajput, R. Mahale, Hand sign interpreter 1, (2012) 19–25.

[102] A.S. Ghotkar, R. Khatal, S. Khupase, S. Asati, M. Hadap, Hand gesture recognition for indian sign language, 4 (2012) 1–4.

[103] G. Saggio, A novel array of flex sensors for a goniometric glove, Sensors Actuators, A Phys. 205 (2014) 119–125. doi:10.1016/j.sna.2013.10.030.

[104] S. Bakhshi, M.H. Mahoor, Development of a wearable sensor system for measuring body joint flexion, Proc. - 2011 Int. Conf. Body Sens. Networks, BSN 2011. (2011) 35–40. doi:10.1109/BSN.2011.20.

[105] G. Saggio, L. Bianchi, S. Castelli, M. Santucci, M. Fraziano, A. Desideri, In Vitro Analysis of Pyrogenicity and Cytotoxicity Profiles of Flex Sensors to be Used to Sense Human Joint Postures, Sensors. 14 (2014) 11672–11681. doi:10.3390/s140711672.

[106] T : The Society for Imaging Science and Technology sole copyright owners of IS Digital fabrication of " smart " structures and mechanisms - creative applications in art and design, (2011).

[107] G. Saggio, Mechanical model of flex sensors used to sense finger movements, Sensors Actuators, A Phys. 185 (2012) 53–58. doi:10.1016/j.sna.2012.07.023.

[108] J.E. Kesner, R.M. Gavalis, P.Y. Wong, C.G.L. Cao, Multifiber optical bend sensor to aid colonoscope navigation, Opt. Eng. 50 (2011) 124402. doi:10.1117/1.3656750.

[109] S. Endler, S. Ferwana, H. Rempp, C. Harendt, J.N. Burghartz, Two-dimensional flex sensor exploiting stacked ultrathin chips, IEEE Electron Device Lett. 33 (2012) 444–446. doi:10.1109/LED.2011.2178389.

[110] J. Zhou, Y. Gu, P. Fei, W. Mai, Y. Gao, R. Yang, et al., Flexible piezotronic strain sensor., Nano Lett. 8 (2008) 3035–40. doi:10.1021/nl802367t.

[111] N. Liu, G. Fang, W. Zeng, H. Long, L. Yuan, X. Zhao, 11 Novel ZnO Nanorod Flexible

Strain Sensor and Strain Driving Transistor with an Ultrahigh 107 Scale “On” -“Off” Ratio Fabricated by a Single-Step Hydrothermal Reaction.pdf, (2011) 570–575.

[112] B. Radha, A.A. Sagade, G.U. Kulkarni, Flexible and semitransparent strain sensors based on micromolded Pd nanoparticle-carbon μ-stripes, ACS Appl. Mater. Interfaces. 3 (2011) 2173–2178. doi:10.1021/am2002873.

[113] L. Lin, S. Liu, Q. Zhang, X. Li, M. Ji, H. Deng, et al., Towards tunable sensitivity of electrical property to strain for conductive polymer composites based on thermoplastic elastomer, ACS Appl. Mater. Interfaces. 5 (2013) 5815–5824. doi:10.1021/am401402x.

[114] S. Ryu, P. Lee, J.B. Chou, R. Xu, R. Zhao, A.J. Hart, et al., Extremely Elastic Wearable Carbon Nanotube Fiber Strain Sensor for Monitoring of Human Motion, ACS Nano. 9 (2015) 5929–5936. doi:10.1021/acsnano.5b00599.

[115] C. Li, Y.-L. Cui, G.-L. Tian, Y. Shu, X.-F. Wang, H. Tian, et al., Flexible CNT-array double helices Strain Sensor with high stretchability for Motion Capture, Sci. Rep. 5 (2015) 15554. doi:10.1038/srep15554.

[116] W. Obitayo, T. Liu, A Review: Carbon Nanotube-Based Piezoresistive Strain Sensors, J. Sensors. 2012 (2012) 1–15. doi:10.1155/2012/652438.

[117] O. Kanoun, C. Müller, A. Benchirouf, A. Sanli, T.N. Dinh, A. Al-Hamry, et al., Flexible carbon nanotube films for high performance strain sensors., Sensors (Basel). 14 (2014) 10042–71. doi:10.3390/s140610042.

[118] E. Roh, B.U. Hwang, D. Kim, B.Y. Kim, N.E. Lee, Stretchable, Transparent, Ultrasensitive, and Patchable Strain Sensor for Human-Machine Interfaces Comprising a

Nanohybrid of Carbon Nanotubes and Conductive Elastomers, ACS Nano. 9 (2015) 6252–6261. doi:10.1021/acsnano.5b01613.

[119] M.A. Darabi, A. Khosrozadeh, Q. Wang, M. Xing, Gum Sensor: A Stretchable, Wearable, and Foldable Sensor Based on Carbon Nanotube/Chewing Gum Membrane, ACS Appl. Mater. Interfaces. 7 (2015) 26195–26205. doi:10.1021/acsami.5b08276.

[120] J.M. Wu, C.-Y. Chen, Y. Zhang, K.-H. Chen, Y. Yang, Y. Hu, et al., Ultrahigh Sensitive Piezotronic Strain Sensors Based on a ZnSnO3 Nanowire/Microwire, ACS Nano. 6 (2012) 4369–4374. doi:10.1021/nn3010558.

[121] M. Kurata, X. Li, K. Fujita, PVDF piezo film as dynamic strain sensor for local damage detection of steel frame buildings, … Struct. …. 8692 (2013) 1–10. doi:10.1117/12.2009554.

[122] Y. Qin, Q. Peng, Y. Ding, Z. Lin, C. Wang, Y. Li, et al., Lightweight, Superelastic, and Mechanically Flexible Graphene/Polyimide Nanocomposite Foam for Strain Sensor Application, ACS Nano. 9 (2015) 8933–8941. doi:10.1021/acsnano.5b02781.

[123] J.S. Lee, K. Shin, O.J. Cheong, J.H. Kim, J. Jang, Highly Sensitive and Multifunctional Tactile Sensor Using Free-standing ZnO / PVDF Thin Film with Graphene Electrodes for Pressure and Temperature Monitoring, Sci. Rep. 5 (2015) 1–8. doi:10.1038/srep07887.

[124] J. Nunes-Pereira, V. Sencadas, V. Correia, V.F. Cardoso, W. Han, J.G. Rocha, et al., Energy harvesting performance of BaTiO3/poly(vinylidene fluoride-trifluoroethylene) spin coated nanocomposites, Compos. Part B Eng. 72 (2015) 130–136. doi:10.1016/j.compositesb.2014.12.001.

[125] M. Sajid, H.W. Dang, K.H. Na, K.H. Choi, Highly stable flex sensors fabricated through mass production roll-to-roll micro-gravure printing system, Sensors Actuators, A Phys. 236 (2015) 73–81. doi:10.1016/j.sna.2015.10.037.

[126] Y. Tang, Z. Zhao, H. Hu, Y. Liu, X. Wang, S. Zhou, et al., Highly Stretchable and Ultrasensitive Strain Sensor Based on Reduced Graphene Oxide Microtubes-Elastomer Composite, ACS Appl. Mater. Interfaces. 7 (2015) 27432–27439. doi:10.1021/acsami.5b09314.

[127] M. Amjadi, M. Turan, C.P. Clementson, M. Sitti, Parallel Microcracks-based Ultrasensitive and Highly Stretchable Strain Sensors, ACS Appl. Mater. Interfaces. (2016) acsami.5b12588. doi:10.1021/acsami.5b12588.

[128] M. Borghetti, M. Serpelloni, E. Sardini, S. Pandini, Mechanical behavior of strain sensors based on PEDOT:PSS and silver nanoparticles inks deposited on polymer substrate by inkjet printing, Sensors Actuators A Phys. 243 (2016) 71–80. doi:10.1016/j.sna.2016.03.021.

[129] M. Park, J. Im, J. Park, U. Jeong, Micropatterned stretchable circuit and strain sensor fabricated by lithography on an electrospun nanofiber mat, ACS Appl. Mater. Interfaces. 5 (2013) 8766–8771. doi:10.1021/am4026032.

[130] M. Amjadi, A. Pichitpajongkit, S. Lee, S. Ryu, I. Park, Highly Stretchable and Sensitive Strain Sensor Based on Silver-Elastomer Nanocomposite, ACS Nano. 8 (2014) 5154–5163.

[131] S. Seyedin, J.M. Razal, P.C. Innis, A. Jeiranikhameneh, S. Beirne, G.G. Wallace, Knitted Strain Sensor Textiles of Highly Conductive All-Polymeric Fibers, ACS Appl. Mater.

Interfaces. 7 (2015) 21150–21158. doi:10.1021/acsami.5b04892.

[132] K.K. Kim, S. Hong, H.M. Cho, J. Lee, Y.D. Suh, J. Ham, et al., Highly Sensitive and Stretchable Multidimensional Strain Sensor with Prestrained Anisotropic Metal Nanowire Percolation Networks, Nano Lett. 15 (2015) 5240–5247. doi:10.1021/acs.nanolett.5b01505.

[133] Q. Liu, M. Zhang, L. Huang, Y. Li, J. Chen, C. Li, et al., High-Quality Graphene Ribbons Prepared from Graphene Oxide Hydrogels and Their Application for Strain Sensors, ACS Nano. 9 (2015) 12320–12326. doi:10.1021/acsnano.5b05609.